Answer to Referee # 1

We thank Anonymous Referee # 1 for their comments. Here below are the Authors' answers point-by-point (in blue) modifications to the text of the manuscript are reported in red.

Page 2, line 3: delete "also"
Deleted
Page 2, line 26: delete "and"
Deleted
Page 4, line 11: replace "and" with "at"
Replaced
Page 4, line 15: "laminar" instead of "linear" (see also page 5, line 16)
Replaced
Page 5, line 29: Lee et al. (2017) is missing in the references
The Referee is correct. We replaced "Lee et al. (2017)" with the correct reference "Lee et al (2018)"
Lee, B. H., Lopez-Hilfiker, F. D., Veres, P. R., McDuffie, E. E., Fibiger, D. L., Sparks, T. L., et al. (2018). Flight Deployment of a High-Resolution Time-of-Flight Chemical Ionization Mass Spectrometer: Observations of Reactive Halogen and Nitrogen Oxide Species. *Journal of Geophysical Research: Atmospheres*. https://doi.org/10.1029/2017JD028082
Page 5, line 30: "l min-1" instead of "liters per minute"
Changed
Page 6, line 5: please check the unit of the mass resolving power (usually expressed as Th/Th and not ppm)
The Referee is correct; the mas resolving power should be expressed in Th/Th. The mass accuracy of the instrument is usually better than 20 ppm. We changed the sentence from "The molecular formulae of the compounds listed above are readily identified given its mass resolving power (4500-5500 ppm (Junninen et al. 2010)..." to "The molecular formulae of the compounds listed above are readily identified given the instrument's mass resolving power (4500-5500 Th Th^{-1} (Junninen et al. 2010)…"
Page 6, line 11: "measure"
Corrected
Page 6, line 19/20: Do the authors mean by uncertainty the standard deviation of the signal at 1 Hz? Can you please also provide a value for the accuracy of the ammonia measurements?
The uncertainty described here refers to the standard deviation of the 1 Hz signal. As it can be indeed misleading, we rephrased this sentence. Systematic errors were minimized by performing frequent backgrounds during flights. We added this information to the manuscript. "The uncertainty of the NH3 measurement during UWFPS was 150 ppt (1σ at 1 Hz sample frequency). To account for potential systematic errors, caused e.g., by changes in cabin temperature, zero measurements were performed regularly during flights "
Page 6, line 27: (i) If the offset at zero NO can be as high as 0.2 ppbv, is there a periodic zero measurement and correction performed? (ii) In this line the units used are pptv and ppbv; before the unit ppt was used, please use pptv consistently
A periodic zero was done for 30 seconds every 5-7 minutes. The text has been changed eliminating the inconsistency in units and adding the remrks from Refereee# 2. "The measurement accuracy was 5% for O_3, NO_x, and NO_2 and 12% for NO_y. Periodic zeros were measured for 30 s every 5-7 min. Measurements were less accurate during periods of rapid altitude change due to a minor pressure dependence in the background zeros in the NO channel that could not be fully corrected during post-processing."
Page 7, line 25: please check the use of the word "when"
Replaced "when" with "with"
Page 7, line 30: "It is . . ."
Corrected
Page 7, line x30-32: since the AMS is not sensitive to particles < _70 nm, can the authors please also comment on the effects the exclusion of these small particles can have
The majority of the mass is in the larger particles. We estimate from SMPS measurements carried out during UWFPS at the William Browning Building on the University of Utah campus site that particle with diameters

smaller than 70 nm contributed to less than 0.5% to the total mass. We changed the sentence from “It also important to note that the term “total nitrate” in this manuscript refers to gas phase plus PM_1 nitrate, but may exclude a non-negligible part of nitrate from the coarse mode.” To “It also important to note that the term “total nitrate” in this manuscript refers to gas phase plus NR-PM_1 nitrate measured with an AMS. While we estimate that particles smaller than 70 nm (lower end of the transmission efficiency of the AMS) contributed to less than 0.5% to the total mass, with our definition we may exclude a non-negligible part of nitrate from the coarse mode.”

Page 8, line 19: remove open bracket

Removed

Page 8, line 26: the green data points (Cache valley) show even higher values (up to 100 μg m-3)

Changed from “During the second pollution episode, the highest aerosol mass concentrations were observed in Utah Valley (~70 μg m-3) and varied for Salt Lake and Cache Valley over the course of the episode (40 – 90 μg m-3)” into “During the first pollution episode, both the aircraft and ground-based aerosol mass concentrations were the highest in Cache Valley (~70 μg m^{-3} and ~90 μg m^{-3} respectively) and the lowest in Utah Valley (~10 μg m^{-3} and ~25 μg m^{-3} respectively). During the second pollution episode, the highest mass concentrations observed at the ground sites in Cache Valley were up to 100 ug m^{-3}, in Utah Valley were ~70 ug m^{-3}, and in Salt Lake Valley were up to 60 ug m^{-3}. These variations among valleys in peak PM2.5 concentrations are characteristic and are due to variations in sources and meteorological processes (Baasandorj et al, 2018) (Figure S2).”

Page 9, line 30: “C2H6”

We changed the sentence from “… showed a contribution from organic fragments, probably CH_2O or C2H6.” To “… showed a contribution from organic fragments.”

Page 10, line 18: “Augsburg”?

Corrected “Augsberg” to “Augsburg”

Page 10, line 21: “compared with”

Corrected

Page 11, line 11: delete “the”

Deleted

Page 11, line 18: “emissions” instead of “concentrations”?

Yes, we replaced “concentrations” with “emissions”

Page 12, line 5: “650 m AGL”

We added “m AGL” after “650”

Page 12, line 24: “divided by”

Corrected

Page 13, line 5: “than in Cache . . .”

Corrected

Page 14, line 20: the 20% contour line seems to be rather yellow-greenish instead of Orange

The referee is correct. We replaced “orange” with “yellow” in the text

Page 14, line 26: I read the figure such that when a counter line intercepts with the maximum value on an axis, both ammonia and nitrate need to be reduced in order to decrease the aerosol loading further. This would be the case for > _60% regarding nitrate.

We agree with the referee. We changed the sentence “However, both reagents must decrease in order to achieve a reduction of total aerosol mass larger than 40% relative to observed conditions.” To “However, both reagents must decrease in order to achieve a reduction of total aerosol mass larger than 60% relative to observed conditions.”

Figure 5: In most figures the unit μg m-3 is being used; it would be good not to switch between units (ppbv and μg m-3)

We changed the units to μg m^{-3}

Figure 7: The agreement between UHSAS and AMS data is generally very good except for the bottom panel on the left. Is there any explanation why the concentrations differ in this profile?

We improved the time alignment for UHSAS and AMS in a new version for Figure 7. The agreement between UHSAS and AMS in the bottom panel is within experimental uncertainties (Figure S6).

SI (1st paragraph on page 1): Can the authors please specify what velocity they are referring to (particle velocity in the sampling line, velocity in the AMS flight chamber, . . .)?

We modified the paragraph by adding the text in red: “Normal procedures were used to calibrate the AMS flow rate as a function of measured lens pressure and particle time-of-flight velocity (i.e. the velocity of the aerosol particles in vacuum, from the chopper to the vaporizer) as a function of particle size [Canagaratna et al., 2007]. For airborne measurements, we used a pressure-controlled inlet (PCI) that maintained a constant mass flow rate into the AMS [Bahreini et al., 2008]. Because particle time-of-flight velocity depends on … the PCI also provided a stable particle time-of-flight velocity calibration.”

Answer to Referee # 2

We thank Anonymous Referee # 2 for their comments. Here below are the Authors' answers point by point)in blue).

In the Introduction (page 3, line 5), the authors write "those studies suggested that nighttime nitrate formation within the residual layer was a major contributor to surface level PM2.5 concentrations." I understood that investigating this type of processes was one of the goals of the campaign. But little is said in the paper about the origin of ammonium nitrate precursors, within the study region, or outside. During winter time, kow qicly HNO3 would be formed from NOx emissions. May be the observational data set does not allow such a discussion, or it is foreseen for another paper. Authors should please state something about that. If the origin within the study region is most important, it would be interesting to show NOx and NH3 emission maps.

The Referee is correct. Identifying the sources was indeed one of the objectives of the UWFPS measurement campaign. However, the scope of this manuscript was to 1) characterize the chemical composition of the aerosol particles and 2) investigate the effects of the decreases of total nitrate and total ammonium in the region. In other words "to achieve a better understanding of the processes that drive the conversion of precursor vapors into aerosol particles," as we wrote in the introduction (page 3 line 26).

Other manuscripts such as Moravek et al., (in preparation) will discuss the sources of NH3 in the region, showing the NH3 emission maps from the inventory and comparing them to the Twin Otter measurements. The paper will focus on NH_3 sources, but will also touch on NOx sources in the region. In addition, a second manuscript by McDuffie et al (in preparation) will investigate the contribution of nocturnal heterogeneous reactive nitrogen chemistry to particulate matter formation. A third paper by Womack et al (under review) explores NOx and VOC control as mitigation strategies for PM. Unfortunately, all these manuscripts are not published yet and therefore not possible to cite properly in the current paper.

The authors state that other cations as Ca2+ or Mg2+ could bound a major part of nitrate. Although this is excluded of total nitrate as defined in the paper, it would be interesting to know what Ca2+ or Mg2+ levels could be typically expected.

We have ion chromatography measurements of gas and aerosol phase at the University of Utah site that show presence of Ca^{2+}, Na^+ and K^+ in $PM_{2.5}$ (Mg^{2+} was always close to the detection limit ~0.01 ug/m^3). The average concentrations were 0.14 $\mu g\ m^{-3}$ (max 1.2 $\mu g\ m^{-3}$) 0.09 $\mu g\ m^{-3}$ (max 3.6 $\mu g\ m^{-3}$) and 0.25 $\mu g\ m^{-3}$ (max 1.6 $\mu g\ m^{-3}$) respectively. The mass fractions of these species were always less than 10% of the total PM2.5 when the PM2.5 was > 20 ug m^{-3}). Ca2+ was always less than 3% and usually less than 1% for the high PM2.5 mass periods. The results of those measurements will be presented in detail in a separate manuscript by Hrdina et al. (in preparation).

How do meteorological conditions affect the isorropia calculated equilibria ? E4xtend the discussion would be interesting. Is aerosol expected to be liquid or solid ?

We agree with the Referee that it would be interesting to explore how the meteorological variables and aerosol phase affect the equilibria from the ISORROPIA model. However, we think that such a discussion is out of the scope of the paper. Cold temperatures and high relative humidity generally favor the formation of ammonium nitrate in the aerosol phase in both the model and our observations. In the area studied during UWFPS the median RH and temperature were 0.66 and 271 K, respectively, and the phase of the aerosol is unknown at these conditions.

In Figure 7b , Salt lake city: The potential temperature profile decreases with altitude. This is not possible in this extent. Are potential temperature and temperature mismatched? In figure 8, another profile is shown.
The referee is correct the temperatures presented in Figures 7 are 8 air temperatures, not potential temperatures. We corrected the labels in both figures. In Figure 8 different profiles are shown because those are averages over polluted periods, not single missed approaches as in Figure 7.

Minor remarks :
Introduction: In Europe Petetin et al., 2016 performed a similar study as the one pre-sented, although based on daily measurements and for an urban environment. This could be cited.
We added the citation

Page 5, line 4 : "It is important to note that refractory species such as sea and / or lake salt (mostly sodium chloride), road salt (mostly magnesium chloride), dust (mostly alkali salts and silicon oxides), and black carbon (from diesel exhaust or wood combustion) are not routinely measured with the AMS" The sentence is not clear. I think you mean that they have not been measured during the campaign.
We changed the sentence into "It is important to note that during the campaign refractory species such as sea and / or lake salt (mostly sodium chloride), road salt (mostly magnesium chloride), dust (mostly alkali salts and silicon oxides), and black carbon (from diesel exhaust or wood combustion) were not measured."

Page 6, line 27: "but zero uncertainty can be as large as 0.2 ppbv" I wonder what are the reasons for this ? Could it be due to HNO3 sticking on inlet walls, and getting desorbed?
The reasons to the uncertainty being so large at times is related to a minor pressure-dependence in the background zeros in the NO channel. We added that information in the text. Inlet effects, such as HNO3 sticking on inlet walls, would not be relevant for the NO, NO2, O3 channels, as those channels are "blind" to HNO3.

Page 8, line 24 "During the first pollution episode, both the aircraft and ground-based aerosol mass concentrations were the highest in Cache Valley (_70 μg m-3) and the lowest in Utah Valley (_10 μg m-3). During the second pollution episode, the highest aerosol mass concentrations were observed in Utah Valley (_70 μg m-3) and varied for Salt Lake and Cache Valley over the course of the episode (40 – 90 μg m-3). During UWFPS, PM2.5 was on average around 70% of PM10 in the three valleys (Figure S3)."
How to explain these differences between valley concentrations for different episodes be explained ?
We added at page 9 line 5: ""These variations among valleys in peak PM2.5 concentrations are characteristic and are due to variations in sources and meteorological processes (Baasandorj et al, 2018) (Figure S2)."
We further modified the prior sentences, taking surface based measurements during non-flight times into account, to: "During the first pollution episode, both the aircraft and ground-based aerosol mass concentrations were the highest in Cache Valley (~70 µg m-3 and ~90 µg m-3 respectively) and the lowest in Utah Valley (~10 µg m-3 and ~25 µg m-3 respectively). During the second pollution episode, the highest mass concentrations observed at the ground sites in Cache Valley were up to 100 ug m-3, in Utah Valley were ~70 ug m-3, and in Salt Lake Valley were up to 60 ug m-3."
Page 8, line 30: Please define Â´n total aerosol mass Â˙z, probably PM1 non-refractive species measured by AMS.
We modified the sentence to "For the purposes of this analysis, we define clean conditions, when the total aerosol mass (NR-PM$_1$) is ≤ 2 µg m^{-3} and …"

Page 9, line 20: "The scatterplot gives an average slope of 1.8 g cm-3, which is comparable to the density of ammonium nitrate (1.72 g cm-3), within the combined measurement uncertainty." But it could be consistent, within the measurement uncertainty, with the density of other aerosol species too, isn't it ?

That is correct. However, ammonium nitrate is mentioned here because it is the largest component of the aerosol as the AMS measurements show.

Page 9, line 23: “Those correspond to measurements in the plume of the U.S. Magnesium plant (Figure S1) where we observed a high organic (74.0±1.2%), high chloride (6±0.6%) and low ammonium mass fraction (3±0.6%).” What are the typical emissions of such a factory ?

The U.S. magnesium plant it is the largest producer of primary magnesium in North America. It has a natural gas power plant on site and a processing plant. According to our measurements, it emits a large amount of aerosols, chloride and other halogens in the gas phase.

Page 13, line 27 “Reduction in total nitrate led to approximately a proportional decrease in total aerosol concentrations during polluted conditions and across all locations.” Is total aerosol or total nitrate meant ?

As written, we meant total inorganic aerosol. We changed the sentence to be more precise into “Reduction in total nitrate led to approximately a proportional decrease in total inorganic aerosol concentrations during polluted conditions and across all locations”

Page 15, line 6 : “The PM2.5 mass loadings for the region varied from below the AMS detection limit of 0.38 to 72.4 µg m-3 (2nd and 98th percentiles).” This suggests that AMS measures PM2.5 or that PM2.5 was derived from AMS. Please clarify from which type of measurement PM2.5 loadings have been calculated here (Surface ?).

The referee is correct. It should be NR-PM_1. We corrected the sentence.

Wording , typos :

Page 2, line 2: “lead” => “leads”

Corrected

Page 5, line 28 : I would say Â´n reactive nitrogen species Â˙z instead of ”nitrogen oxides Â˙z. oxide

We decided to leave the sentence unchanged, as by using “reactive nitrogen species” the sentence would result less specific.

Page 8, line 19: Please correct Â´n (, which is surrounded Â˙z

Corrected

Page 9, line 30: Â´n C2H6 Â˙z plus put indices.

We changed the sentence from “… showed a contribution from organic fragments, probably CH_2O or C2H6.” To “… showed a contribution from organic fragments.”

Page 11, line 33 : Â´n slightly Â˙z => “slight”

Corrected

References

Baasandorj, M., Brown, S. S., Hoch, S., Crosman, E., Long R., Silva, P. Mitchell L., Hammond I., Martin, R., Bares R., Lin, J., Sohl J.,Page, J., McKeen, S., Pennell, C., Franchin, A., Middlebrook, A., Petersen, R., Hallar, G., Fibiger, D., Womack, C., McDuffie, E., Moravek, A., Murphy, J., Hrdina, A., Thornton, J., Goldberger, L., Lee, B., Riedel, T., Whitehill, A., Kelly, K., Hansen, J., Eatough, D., 2017 Utah Winter Fine Particulate Study Final Report, 2017.https://www.esrl.noaa.gov/csd/groups/csd7/measurements/2017uwfps/finalreport.pdf (Last accessed June 2018)

Airborne and ground-based observations of ammonium nitrate dominated aerosols in a shallow boundary layer during intense winter pollution episodes in northern Utah

Alessandro Franchin[1,2], Dorothy L. Fibiger[1,2,Δ], Lexie Goldberger[3,*], Erin E. McDuffie[1,2], Alexander Moravek[4], Caroline C. Womack[1,2], Erik T. Crosman[5], Kenneth S. Docherty[6], William P. Dube[1,2], Sebastian W. Hoch[5], Ben H. Lee[3], Russell Long[7], Jennifer G. Murphy[4], Joel A. Thornton[3], Steven S. Brown[1], Munkhbayar Baasandorj[5], and Ann M. Middlebrook[1]

[1]NOAA Earth System Research Laboratory (ESRL) Chemical Sciences Division, 325 Broadway, Boulder, CO 80305, USA
[2] Cooperative Institute for Research in Environmental Sciences (CIRES), University of Colorado, Boulder, CO 80309, USA
[3] University of Washington, Department of Atmospheric Sciences, Seattle, WA 98195, USA
[4] Department of Chemistry, University of Toronto, Toronto, ON, M5S 3H6, Canada
[5] University of Utah, Department of Atmospheric Sciences, Salt Lake City, UT 84112, USA
[6] Jacobs Technology, Inc., RTP, NC 27709, USA
[7] Environmental Protection Agency (EPA), Durham, NC 27709, USA
[,Δ] Now at California Air Resources Board, Monitoring and Laboratory Division, Sacramento, CA 95811, USA.
[*] Now at Pacific Northwest National Laboratory, Richland, WA 99354, USA.

Correspondence to: Alessandro Franchin (alessandro.franchin@noaa.gov)

Abstract. Airborne and ground-based measurements of aerosol concentrations, chemical composition and gas phase precursors were obtained in three valleys in northern Utah (U.S.A.). The measurements were part of the Utah Winter Fine Particulate Study (UWFPS) that took place in January-February, 2017. Total aerosol mass concentrations of PM$_1$ were measured from a Twin Otter aircraft, with an Aerosol Mass Spectrometer (AMS). PM$_1$ concentrations ranged from less than 2 μg m^{-3} during clean periods to over 100 μg m^{-3} during the most polluted episodes, consistent with PM$_{2.5}$ total mass concentrations measured concurrently at ground sites. Across the entire region, increases in total aerosol mass above ~ 2 μg m^{-3} were associated with increases in the ammonium nitrate mass fraction, clearly indicating that the highest aerosol mass loadings in the region were predominantly attributable to an increase in ammonium nitrate. The chemical composition was regionally homogenous for total aerosol mass concentrations above 17.5 μg m^{-3}, with 74±5% (average ± standard deviation) ammonium nitrate, 18±3% organic material, 6±3% ammonium sulfate, and 2±2% ammonium chloride. Vertical profiles of aerosol mass and volume in the region showed variable concentrations with height in the polluted boundary layer. Higher average mass concentrations were observed within the first few hundred meters above ground level in all three valleys during pollution episodes. Gas phase measurements of nitric acid (HNO$_3$) and ammonia (NH$_3$) during the pollution episodes revealed that in Cache and Utah Valley, partitioning of inorganic semi-volatiles to the aerosol phase was usually limited by the amount of gas phase nitric acid, with NH$_3$ being in excess. The inorganic species were compared with the ISORROPIA thermodynamic model. Total inorganic aerosol mass concentrations were calculated for various decreases of total nitrate and total ammonium.

For pollution episodes, our simulations of a 50% decrease in total nitrate leads to a 46±3% decrease in total PM_1 mass. A simulated 50% decrease in total ammonium leads to a 36±17% μg m^{-3} in total PM_1 mass, over the entire area of the study. Despite some differences among different locations, our results ~~also~~ showed a higher sensitivity to decreasing nitric acid concentrations and the importance of ammonia at the lowest total nitrate conditions. In the Salt Lake Valley, both HNO_3 and NH_3 concentrations controlled aerosol formation.

1 Introduction

Intense wintertime air pollution from particulate matter affects numerous locations in the United States (Chen et al., 2012; *Lurmann et al.*, 2006) and around the world (Bessagnet et al.,2005; Gwaze et al., 2007; Petetin et al., 2016, Ricciardelli et al., 2017; Wang et al., 2014). In the U.S., pollution from fine particles ($PM_{2.5}$) has been decreasing in the past decades. However, $PM_{2.5}$ concentrations in Salt Lake City and surrounding valleys remain among the highest nationwide (EPA, 2017). High $PM_{2.5}$ episodes in these areas occur predominantly during winter, when persistent cold-air pools (PCAPs) form as a result of high-pressure ridges (Whiteman et al. 2014, Lareau et al. 2013). These events increase in frequency and severity during snow covered periods (Green et al., 2015). Under PCAP conditions, emissions of pollutants and precursor gases are trapped in a shallow boundary layer, as vertical mixing is limited. Precursor gases react chemically, increasing the production of $PM_{2.5}$ via secondary pathways. Almost every year, wintertime concentrations of $PM_{2.5}$ exceed the limit of 35 μg m^{-3} in a 24 h average in the Logan, Ogden-Clearfield, Salt Lake City and Provo-Orem Core-Based Statistical Areas (CBSAs, EPA Air Quality Statistics by City, 2016), leading to violations of the National Ambient Air Quality Standards (NAAQS) set by the Environmental Protection Agency (EPA). This air quality issue affects almost 80% of the population of the state of Utah, and has been associated with increased risk for stroke, heart disease, lung cancer, and both chronic and acute respiratory diseases [*Beard et al.*, 2012; *Pope et al.*, 2006, WHO, 2016].

Chemical composition measurements of PM and their precursor gases, together with a detailed understanding of the meteorology are key to identifying sources and developing mitigation strategies. Previous studies showed that ammonium nitrate (NH_4NO_3) dominates the aerosol mass during pollution episodes (Hansen et al., 2010; Kelly et al., 2013; Kuprov et al., 2014; Long et al., 2003; Long et al., 2005a; Long et al., 2005b; Mangelson et al.,1997; Silva et al., 2007). Analysis of ground-based data suggests ~~and~~ that its formation, at least in the Salt Lake Valley and Cache Valley is likely to be nitric acid limited (Kuprov et al., 2014; Mangelson et al., 1997). The Great Salt Lake is a potential source of chloride in the area, and chloride may also play a role during pollution episodes, although its role is much less clear. Hansen and co-workers found chloride (in the form of sodium chloride) to be a minor part of the $PM_{2.5}$ mass fraction (1.3% on average over the period of their study January 22–31, 2007 in Lindon, UT; Hansen et al., 2010). However, Kelly and co-workers, using two different factor analysis techniques, found that, after ammonium nitrate, ammonium chloride could also be a significant source of secondary wintertime $PM_{2.5}$ (Kelly et al., 2013).

Formation of $PM_{2.5}$ results in part from a complex interaction of chemical production mechanisms with boundary layer meteorology (Baasandorj et al., 2017a). Previous studies carried out in wintertime in San Joaquin Valley (CA) highlighted the critical role of nocturnal chemical production of nitrate aloft in the residual layer (i.e. that region decupled from the stable nocturnal boundary layer influenced by previous day surface emissions). Those studies suggested that nighttime nitrate formation within the residual layer was a major contributor to surface-level $PM_{2.5}$ concentrations (Watson et al., 2001; Brown et al., 2006; Chow et al., 2006; Lurmann et al., 2006, Prabhakar et al., 2017). Studies in other regions of the U.S. have reached similar conclusions regarding the role of nighttime processing aloft as a source of winter soluble nitrate (Stanier et al., 2012; Kim et al., 2014). Similarly, Baasandorj and co-workers found evidence in their ground-based observations in the Salt Lake City area for nitrate formation occurring at night and early morning photochemistry in the upper levels of a PCAP (Baasandorj et al., 2017a). Although the residual layer is inferred to be a critical region for understanding process level atmospheric chemistry leading to winter ammonium nitrate in polluted regions, few air quality studies have directly probed residual layer chemical composition using an instrumented aircraft in a polluted winter boundary layer (Brown et al., 2013, McDuffie et al., 2018).

In this work, we present results of the Utah Winter Fine Particulate Study (UWFPS), an intensive measurement campaign combining airborne and surface-based measurements that took place in Salt Lake City and surrounding valleys in January and February 2017 (Figure 1 and Figure S1). In particular, we focus on the chemical and physical aerosol properties measured by an aerosol mass spectrometer (AMS) and an ultra-high sensitivity aerosol spectrometer (UHSAS) aboard the National Oceanic and Atmospheric Administration (NOAA) Twin Otter research aircraft. The flights took place from January 16th to February 12th and were based out of the Salt Lake City International Airport, with flight plans extending up to Cache Valley, across the Great Salt Lake, and over the Salt Lake and Utah Valleys. Flight plans included missed approaches at several local airports in the three main study regions to probe the vertical structure of the concentrations of aerosols and precursor gases. The NOAA Twin Otter aircraft was equipped with a suite of instruments that allowed comprehensive measurements of the aerosols and the gas phase precursors that contribute to the pollution episodes in the area.

The goal of this analysis is to achieve a better understanding of the processes that drive the conversion of precursor vapors into aerosol particles. We compared measured inorganic gas and particle composition to a thermodynamic model and used the model output to probe sensitivities to changes in that composition that are useful to developing effective $PM_{2.5}$ control strategies.

2 Methods

The airborne measurements, carried out using the NOAA Twin Otter aircraft, were designed to characterize pollution episodes with a particular focus on ammonium nitrate aerosol formation. The aerosol measurements from the aircraft were compared with ground-site data of $PM_{2.5}$, PM_{10}, and non-refractory PM_1 (NR-PM_1) obtained by the Utah Department of Air Quality (UDAQ) and the U. S. Environmental Protection Agency (EPA). The thermodynamic model ISORROPIA was used to compare predicted aerosol to vapor partitioning with the measurements.

2.1 Twin Otter Aircraft Instrumentation

2.2.1 Aerosol Measurements

Aerosols were sampled using a perpendicular near-isokinetic inlet described and characterized previously for aircraft measurements (Perring et al., 2013). The inner diameter of the secondary diffuser of the inlet was modified from the original inlet (Ø=2.5 mm in the modified version) to accommodate a 3 liter per minute (l min^{-1}) total inlet flow ~~and~~ at the lower cruise speed of the Twin Otter (~250 km h^{-1}). The total inlet flow was chosen in order to limit sampling line losses due to diffusion and evaporation. The sampled air downstream of the inlet probe was split into a 37 cm sampling line to the UHSAS and a 153 cm sampling line to the AMS with an excess flow of about 2.8 l min^{-1} that was discarded. The excess flow was monitored with a ~~linear~~ laminar flow element and a calibrated pressure transducer (Honeywell 480-5439-ND).

The Aerosol Mass Spectrometer (AMS, Aerodyne Research Inc., Billerica, MA) measures the chemical composition of the non-refractory aerosol particles in the 70 to 850 nm range (NR-PM_1) (Canagaratna et al., 2007; Drewnick et al., 2005; Jayne et al., 2000). The working principle of the AMS is to 1) focus ambient aerosols in a vacuum chamber with an aerodynamic lens, 2) evaporate the aerosol particles by impacting them onto a 600 °C surface, and 3) ionize the evaporated molecules with electron-impact ionization and analyze the resulting fragments with a mass spectrometer to obtain information on the chemical composition of aerosols. For the majority of sampling, the AMS collected bulk mass spectra (MS mode). Additionally, aerosol size distributions are obtained by operating the AMS in particle time of flight (pToF) mode wherein mass spectrometer signals are monitored as a function of the time required for particles of different sizes to traverse the length of the vacuum chamber. The NOAA AMS deployed on the Twin Otter aircraft (TO-AMS) was equipped with a pressure-controlled inlet to maintain a constant mass flow rate into the instrument as the aircraft changed altitude (Bahreini et al., 2008). The TO-AMS was also equipped with a light scattering module (LS) that provided a more accurate size information in the range 200-1000 nm and on the collection efficiency (Liao et al., 2017). A CE of 1 was used for this analysis based on the light scattering (see SI).

The TO-AMS was operated in MS mode (6 seconds, with 4 s open to sample and 2 s closed for background correction) and pTOF mode (4 seconds) in 27 sub-cycles of 10 seconds total. We measured in LS mode for 30 seconds every 4.5 minutes. The aircraft AMS measurements are all reported in units of micrograms per standard cubic meter of air, where standard conditions are 273 K and 1 atm. Details of the AMS calibration procedures for the UWFPS are presented in the SI. The 10 s average limit of detection for nitrate (NO_3^-), ammonium (NH_4^+), organic species (Org), sulfate (SO_4^{2-}), chloride (Cl^-) and for the total aerosol mass were 0.04, 0.09, 0.33, 0.03, 0.07, and 0.38 µg m^{-3} respectively. The uncertainty in the total AMS mass concentrations is estimated to be 20% (Bahreini et al., 2009). ~~It is important to note that refractory species such as sea and / or lake salt (mostly sodium chloride), road salt (mostly magnesium chloride), dust (mostly alkali salts and silicon oxides), and black carbon (from diesel exhaust or wood combustion) are not routinely measured with the AMS.~~ It is important to note that during the campaign refractory species such as sea and / or lake salt (mostly sodium chloride), road salt (mostly magnesium chloride), dust (mostly alkali salts and silicon oxides), and black carbon (from diesel exhaust or wood combustion) were not measured.

The Ultra-High Sensitivity Aerosol Spectrometer (UHSAS, Droplet Measurement Technologies, Longmont, CO) was used to measure the dry size distributions of aerosol particles in the range of 70 to 1000 nm. The working principle of the UHSAS is based on optical-scattering. The aerosol particles enter the instrument and scatter the light produced by a solid-state laser (1054 nm, 1 kW/cm^2). Mirrors capable of collecting light over a large solid angle (22°–158°) direct the scattered light to two different photodiodes: an avalanche photodiode for detecting the smallest particles and a low-gain PIN photodiode for detecting particles in the upper size range. The signals generated by the scattered light are used for particle sizing since the amount of light scattered correlates strongly with particle size (Cai et al., 2008). UHSAS data during the UWFPS were recorded every 3 sec and are reported here per standard cubic centimeter (273 K and 1 atm). The relative humidity in the sampling line was calculated to be less than 30%. The UHSAS inlet flow was monitored with a linear flow element and a calibrated pressure transducer Honeywell 480-5439-ND) in order to correct for variations in the inlet flow (Brock et al., 2011). The uncertainty during UWFPS was 2% on the sizing, 14% on the number concentration, 20% on the total surface and 35% on the total volume.

2.2.2 Gas Phase Measurements

On the Twin Otter aircraft, we obtained measurements of several gas phase species, including those relevant for inorganic gas-aerosol partitioning in the region: nitric acid (HNO_3), hydrochloric acid (HCl), and ammonia (NH_3). We used these aircraft gas phase species, as well as data from aerosol phase nitrate, chloride, and ammonium to calculate the ratios of gas over the total ammonium or total nitrate for estimating which species is the limiting reagent in ammonium nitrate formation and for the input to thermodynamic modeling with ISORROPIA (see section 2.3).

The University of Washington high-resolution time-of-flight iodide adduct ionization mass spectrometer, hereafter referred to as HRToF-CIMS, was used to measure a suite of reactive inorganic gaseous halogen (HCl, Cl_2, Br_2, $ClNO_2$, etc.) and nitrogen oxide (HNO_3, N_2O_5, HONO, etc.) species. The major components of the CIMS were described previously (Lee et al., 2014) with upgrades implemented prior to UWFPS to improve in-flight calibration and sampling protocol (Lee et al., ~~2017~~2018). Ambient air was drawn in to the CIMS at a rate of ~22 ~~liters per minute~~l min^{-1} through a 39 cm long 1.6 cm inner diamter (ID) polytetrafluoroethylene (PTFE) inlet, resulting in a mean residence time of about ~0.21 seconds. The CIMS instrument subsamples 2 slpm from the centerline of the main flow traveling through the 1.6 cm ID inlet with the remainder of the flow being pulled radially through a circular slot around and downstream of the ion molecule reaction (IMR) region entrance, to minimize sampling air that has been in contact with the inlet surface. Instrument background levels were determined every 60 seconds for a duration of 5 seconds by overflowing the IMR with ultra high purity nitrogen (UHP N_2). The UHP N_2 was introduced at the entrance of the IMR region, which represents the dominant source (>80%) of the sum of the background levels originating from the inlet and IMR region under field conditions. The molecular formulae of the compounds listed above are readily identified given its mass resolving power (4500-5500 ~~ppm~~ Th Th^{-1} (Junninen et al. 2010), with no known spectrally interfering species. For nitric acid (HNO_3) and hydrogen chloride (HCl), the calibration uncertainty for both is about 30%, while their limits of detection (LOD), determined by accounting for their calibration coefficients and variabilities in their background levels were 60 and 160 ppt, respectively.

A Continuous-Wave Quantum Cascade Tunable Infrared Laser Differential Absorption Spectrometer (QC-TLDAS, Aerodyne Research Inc., Billerica, MA; Tevlin et al 2017) was used to measure~~d~~ ammonia (NH_3) concentrations from the Twin Otter aircraft. Prior to installation, the instrument was optimized for a lower total weight allowing its operation on the Twin Otter aircraft. Furthermore, it was equipped with a pressure control system to account for changing ambient pressure with altitude. Ambient air was aspirated at a flow rate of 4 l min^{-1} through the multi-pass absorption cell (0.5 l, 76 m effective path length) and NH_3 absorption was detected at 965.3 cm^{-1}. In order to minimize adsorption of ammonia on the inlet walls, an additional bypass flow rate of 16 l min^{-1} was introduced to purge the 50 cm long inlet tubing. In addition, the inlet was heated to approximately 40°C to further reduce tubing wall effects. Evaporation of ammonia from NH_4NO_3 aerosols was minimized by removing the particulate matter using a PFA (Teflon) virtual impactor upstream of the QC-TILDAS absorption cell. ~~The uncertainty of the QC-TLDAS during UWFPS was 150 ppt (1σ)~~ The uncertainty of the NH_3 measurement during UWFPS was 150 ppt (1σ at 1 Hz sample frequency). To account for potential systematic errors, caused e.g. by changes in cabin temperature, zero measurements were performed regularly during flights~~.~~ The limit of detection (3σ) was 450 ppt at the 1 Hz sample frequency and 90 ppt for a 30 s averaging interval.

Nitrogen oxides (NO, NO_2) total reactive nitrogen (NO_y) and ozone (O_3) were measured at 1 second time resolution using the NOAA custom-built, nitrogen oxide cavity ring down spectrometer (NOxCaRD). The instrument directly measures NO_2 by optical absorption at 405 nm, and quantitatively converts NO and O_3 into NO_2 by reaction with excess O_3 or NO, respectively, in two separate channels (Fuchs et al., 2009; Washenfelder et al.,2011). A fourth channel converts NO_y to NO and NO_2 by thermal dissociation in a quartz inlet at 650 °C and subsequently converts any NO to NO_2 in excess O_3 (Wild et al., 2014). ~~The measurement precision is 50 pptv or better, but zero uncertainty can be as large as 0.2 ppbv~~The measurement accuracy was 5% for O_3, NO_x, and NO_2 and 12% for NO_y. Periodic zeros were measured for 30 s every 5-7 min. Measurements were less accurate during periods of rapid altitude change due to a minor pressure dependence in the background zeros in the NO channel that could not be fully corrected during post-processing.~~.~~

2.2.3 Meteorological parameters

A commercial met probe (Avantech) measured meteorological parameters (ambient temperature, pressure, relative humidity with respect to liquid water, wind speed and wind direction), the global positioning satellite (GPS) location including altitude above sea level, and aircraft parameters (heading, pitch, and roll). Wind data were compromised for some flights, making only partial coverage available. The aircraft GPS altitude above sea level was converted into altitude above ground level using USGS data (https://gis.utah.gov/data/elevation-and-terrain/).

2.2 $PM_{2.5}$ ground-based measurements

As part of the Utah air monitoring network, UDAQ continually monitors $PM_{2.5}$, PM_{10}, nitrogen oxides or NO_x (NO and NO_2), ozone (O_3) and meteorological parameters according to EPA guidelines and operates 24-h Federal Reference Method (FRM) samplers for $PM_{2.5}$ for NAAQS compliance. Here, we used $PM_{2.5}$ data from two UDAQ sites: Hawthorne, the main air monitoring station for Salt Lake City (40.734397N, 111.8721W), situated on the Salt Lake Valley floor at ~ 1306 m above sea level (ASL) and North Provo (40.253826N, 111.663311W), situated in a central location of the Utah Valley at ~ 1402 m ASL. We also used $PM_{2.5}$ and NR-PM_1 data obtained by the EPA at a temporary sampling station located in Logan (41.758875N, 111.815122W), on the Utah State University campus in the Cache Valley at ~ 1405 m ASL. These three sites are located in three sub-basins in proximity of the Great Salt Lake, in northern Utah.

2.3 Thermodynamic calculations using ISORROPIA

Cold temperatures and the presence of both nitric acid and ammonia are conducive to forming ammonium nitrate in the aerosol phase. To examine phase partitioning of these compounds for the flight data, we used the thermodynamic model ISORROPIA (v2.1) (Fountoukis and Nenes, 2007; Nenes et al., 1998). We run ISORROPIA in "forward" mode, in which the total (gas + particulate) measured concentrations of various inorganic species are input into the model along with meteorological data (temperature and relative humidity). From these input parameters, concentrations for each phase are calculated using the van't Hoff equation assuming thermodynamic equilibrium. The Kelvin effect is neglected in the model calculations and all the aerosol particles are assumed to have the same composition.

The inorganic species used for input to ISORROPIA were simplified here to the available flight data for total nitrate (HNO_3+NO_3^-), total ammonium (NH_3+NH_4^+), total chloride (HCl+Cl^-), and sulfate (SO_4^{2-}). The composition of the particle phase (NO_3^-, NH_4^+ and SO_4^{2-}) was from the TO-AMS, therefore NR-PM_1. As the AMS does not quantitatively measure refractory sodium or its salts (e.g., sodium chloride, nitrate, or sulfate) under normal operating conditions, the model input for particulate sodium was set to zero with the assumption that this does not affect the partitioning of the acidic gases ~~when~~ with their corresponding ammonium salts. In other words, the equilibrium vapor pressures of the inorganic acids examined here are constrained only by their ammonium salts and the vapor pressures of the acidic gases over their sodium salts are considered to be negligible. Because nitric acid is known to displace chloride from sodium, potassium, calcium, and magnesium salts (Bondy et al., 2017; Metzger et al.; 2006; Sudheer and Rengarajan, 2015; Trebs et al., 2005), aerosols containing these refractory species could act as a sink for HNO_3 and source of HCl in this environment. ~~It also important to note that the term “total nitrate” in this manuscript refers to gas phase plus PM_1 nitrate, but may exclude a non-negligible part of nitrate from the coarse mode.~~ It also important to note that the term “total nitrate” in this manuscript refers to gas phase plus NR-PM1 nitrate measured with an AMS. While we estimate that particles smaller than 70 nm (lower end of the transmission efficiency of the AMS) contributed to less than 0.5% to the total mass, with our definition we may exclude a non-negligible part of nitrate from the coarse mode

The ISORROPIA output was compared directly with UWFPS measurements. We then performed several simulations designed to test the model response to decreasing the total nitrate and/or ammonium in order to simulate how much a reduction in total nitrate and/or total ammonium would affect the total aerosol mass. When we compared the total NR-PM_1 mass at different conditions, we used only the inorganic mass, as we did not have enough information on to the organic constituents to include them in the model.

3 Measurement results

3.1 Comparison of ground sites and airborne observations

The UWFPS field intensive measurement period encompassed two complete major pollution episodes (Episode #1 and #2) and the beginning of a third minor pollution episode (Episode #3, Figure 2, left). All of the three ground sites: Logan, in Cache Valley; Hawthorne, in Salt Lake Valley and North Provo, in Utah Valley showed similar increases in $PM_{2.5}$ mass concentrations as a function of time. However, we observed some slight differences that are probably related to the availability of precursor gases and oxidants at the three sites as well as the various basin topographical and meteorological features (Baasandorj et al., 2017a).

The 2016/17 winter had several multi-day pollution episodes and the $PM_{2.5}$ temporal evolution of each individual episode during the UWFPS study period was similar to those from past years (Figure S2). $PM_{2.5}$ levels in the Salt Lake Valley (SLV, in red) often reach a plateau after an initial increase regionally, whereas $PM_{2.5}$ concentrations continue to increase in Utah and Cache Valleys as long as the PCAP persists. Often a PCAP erodes first in Utah Valley and persists the longest in Cache Valley ~~(~~, which is surrounded by mountains and sheltered more effectively from mixing induced by large-scale winds. Similar changes in aerosol mass and volume as a function of time were also observed with the aircraft instruments over the study region. TO-AMS NR-PM_1 measurements near the ground sites (within 8 horizontal km and altitudes less 50 m above ground level, AGL) during the study period correlated well (R^2=0.82) with the $PM_{2.5}$ ground site data measured at the same time and agreed within the measurement uncertainties (Figure 2, right). Hence, aerosol measurements from the aircraft were representative of and consistent with the ground observations. During the first pollution episode, both the aircraft and ground-based aerosol mass concentrations were the highest in Cache Valley (~70 µg m^{-3}~~)~~ and ~90 µg m^{-3} respectively) and the lowest in Utah Valley (~10 µg m^{-3}~~)~~ and ~25 µg m^{-3} respectively). ~~During the second pollution episode, the highest aerosol mass concentrations were observed in Utah Valley (~70 µg m^{-3}) and varied for Salt Lake and Cache Valley over the course of the episode (40 – 90 µg m^{-3}).~~ During the second pollution episode, the highest mass concentrations observed at the ground sites in Cache Valley were up to 100 ug m^{-3}, in Utah Valley were ~70 ug m^{-3}, and in Salt Lake Valley were up to 60 ug m^{-3}. These variations among valleys in peak PM2.5 concentrations are characteristic and are due to variations in sources and meteorological processes (Baasandorj et al, 2018) (Figure S2). During UWFPS, PM$_{2.5}$ was on average around 70% of PM$_{10}$ in the three valleys (Figure S3).

3.2 Aerosol chemical composition during polluted and clean conditions

For the purposes of this analysis, we define clean conditions, when the total aerosol mass (NR-PM$_1$) is ≤ 2 µg m^{-3} and polluted conditions when the total aerosol mass is > 17.5 µg m^{-3}. Our definition of polluted conditions follows the classification used by Whitemann et al. (2014) that links a total aerosol mass > 17.5 µg m^{-3} to PCAP conditions. NR-PM$_1$ composition differed substantially between polluted and clean conditions (Figure 3). During polluted conditions (44% of the Twin Otter data) the dominant species was ammonium nitrate (74±5%, mean ± standard deviation), while organic, sulfate (mostly ammonium sulfate), and chloride (in the form of ammonium chloride) constituted a minor fraction of the mass (18±3%, 6±3%, and 2±2%, respectively). The largest aerosol mass concentrations of ammonium nitrate occurred at temperatures below the ice frost point. During clean conditions (56% of the data), the organic fraction dominated the mass of the aerosols (50±13%), ammonium nitrate was the second most abundant species (31±9%) followed by ammonium sulfate and chloride (13±7% and 6±6% respectively). During pollution episode #2, we observed at ground level an average increase of PM$_{2.5}$ over time of about 11 µg m^{-3} day^{-1}. The increase due to aerosol phase ammonium nitrate was 8.2±0.4 µg m^{-3} day^{-1}, and the remaining contribution of 2.8±0.1 µg m^{-3} day^{-1} was due to the other chemical species according to the mass fractions indicated above. Furthermore, the change in chemical composition was uniform across the three different valleys (Figure 4) and across all other areas in the studied region (Figure S4) both for airplane and for ground-based measurements (Figure S5), although detailed ground-based composition measurements were limited to the site in the Cache Valley. We can therefore say that aerosol mass concentrations were predominantly due to growth in ammonium nitrate across the entire region. This uniformity occurs despite heterogeneity in emissions, with relatively large urban emissions from Salt Lake City and relatively large agricultural emissions in the Cache Valley.

A comparison of the total aerosol mass measured with the AMS with the dry aerosol volume measured with the UHSAS is shown in Figure S6. The scatterplot gives an average slope of 1.8 g cm^{-3}, which is comparable to the density of ammonium nitrate (1.72 g cm^{-3}), within the combined measurement uncertainty. The aerosol-phase ion balance (Figure 5) shows that the aerosols were completely neutralized, indicating that the measured nitrate, sulfate and chloride are predominantly in the form of their corresponding ammonium salts (ammonium nitrate, ammonium sulfate, and ammonium chloride). The data points in orange have a low ammonium nitrate mass fraction and are below the 1:1 line (more acidic). Those correspond to measurements in the plume of the U.S. Magnesium plant (Figure S1) where we observed a high organic (74.0±1.2%), high chloride (6±0.6%) and low ammonium mass fraction (3±0.6%). It is important to note that those AMS measurements of the U.S. magnesium plume reported in the current dataset carry a larger uncertainty than the rest of the dataset. The organic component of the aerosol mass was high (up to 50 µg m^{-3}) and it is likely to be underestimated as CE = 1 was used (CE is < 1 for aerosols that are not ammonium nitrate and usually assumed = 0.5 for organic aerosol). In the plume, the reported nitrate mass is over estimated as the peak at m/z = 30, that is normally attributed to the NO fragment, showed a contribution from organic fragments~~, probably CH_2O or C2H6~~. The plume presented a high aerosol chloride mass, in the form of ammonium chloride at concentrations up to 3.9 µg m^{-3}.

3.3 Contribution of residential wood combustion to the aerosol mass and other organic aerosol sources to the total aerosol mass

Figures 3 and 4 show that the mass fraction of organic material in the particulate phase on a regional basis was generally less than 20% during polluted conditions. There are very few data points in these aircraft observations containing higher organic mass fractions at the highest aerosol mass concentrations, which is consistent with sources of wood combustion organic aerosol varying widely (Shrivastava et al., 2007; Kleindienst et al., 2010; Woody et al., 2016). Hence, this organic aerosol fraction of roughly 20% places an upper limit on the average direct contribution (i.e., from primary aerosol emissions or formation of secondary organic aerosol from wood combustion VOCs) of wood combustion to the regional total aerosol mass.

The organic signals in the mass spectra were examined to further estimate the contribution from wood combustion. Prior studies using an AMS instrument indicate that a potential marker of wood combustion is signal at the mass-to-charge ratio (*m/*z) of 60, which is a major ion fragment present in spectra from the known biomass burning marker species, levoglucosan (Alfarra et al., 2007). The fraction of the organic mass spectrum that is at *m/z* 60 (termed f_{60}) is about 8% in spectra from levoglucosan (Alfarra et al., 2007) and is often significantly larger than the background value of 0.3% (or 0.003) for air masses that are influenced by biomass burning (Cubison et al., 2011). During wintertime evenings, wood combustion is known to be a major contributor to the measured aerosol mass in several European suburban/urban sites, where f_{60} was measured on average to be 0.028 in Roveredo, Switzerland (Alfarra et al., 2007), 0.02 in Grenoble, France (Favez et al., 2010), and slightly less than 0.02 in ~~Augsberg~~Augsburg, Germany (Elasser et al., 2012). Here we measured a median value (with 25th and 75th percentile) for f_{60} of 0.0035 (0.0031 – 0.0042) for the entire study during all conditions, indicating that the contribution of wood combustion to the organic mass fraction was generally fairly low compared to the European sites. The lower panel of Figure 6 shows the distribution of f_{60} for this study (light red) compared with previous studies where the influence of biomass burning was negligible (green, blue and dark red lines). Most of the spectra from our study had f_{60} close to the background value of 0.003, however the distribution shows a somewhat higher tail for our f_{60} values (17% of the data). By comparing with the average fractions from the European wintertime studies, we estimate that the fraction of organic aerosol from wood combustion in these higher f_{60} cases was about 30% of the total organic mass, i.e., about 6% of the total NR-PM$_1$.

Low values of f_{60} could be due to the initial wood combustion aerosol emissions having low f_{60} (Heringa et al., 2012; Schneider et al., 2006) or aging in the atmosphere causing f_{60} to decrease (Corbin et al., 2015; Ortega et al., 2013) before the aerosol was measured on the aircraft. Hence, relatively higher signals from aged aerosols could potentially indicate conversion of the fresh, primary biomass burning aerosols to lower f_{60} due to aging. The common marker for aged, oxidized organic aerosols is the peak at *m/z* 44, which corresponds to the CO_2^+ fragment (Allan et al., 2004). *m/z* 44 correlates with the elemental oxygen/carbon ratio (O:C) (Aiken et al., 2007, 2008; Canagaratna et al., 2015), and indicates organic aerosol aging (Ng et al., 2010; Cubison et al., 2011). A plot of f_{44} (i.e., the ratio of *m/z* 44 to the total organic aerosol mass) versus f_{60} for our study is shown along with Cubison and co-workers' previous data in the upper panel of Figure 6. The data of freshly emitted biomass burning aerosols shown in Cubison et al. (2011) tended to have high f_{60} (0.02 to 0.04) with relatively low f_{44} (about 0.05) that changed to lower f_{60} (<0.02) and higher f_{44} (0.15 to 0.23) as the aerosols aged. For the UWFPS study, however, f_{60} was generally low and f_{44} varied considerably.

Since f_{44} was not consistently high, the organic aerosol was not always highly oxidized, indicating that peaks other than *m/z* 60 were possibly important in the organic aerosol for the UWFPS dataset. Another marker to consider is f_{57} (ratio of *m/z* 57 to the total organic signal in the AMS) which corresponds to a characteristic fragment from hydrocarbon-like organic aerosol (HOA) from lubricating oil and/or diesel fuel and related to traffic emissions (Canagaratna et al., 2004; Zhang et al., 2005). We observed f_{57} median values of 0.009, 0.012 and 0.010 for Cache, Salt Lake and Utah Valley, respectively. The reported f_{57} for the New York City diesel bus exhaust~~-~~ in Canagaratna et al. (2004) and for the Pittsburgh HOA in Zhang et al. (2005) was 0.081 and 0.075, respectively. This indicates that ~~the~~ some of the organic fraction of NR-PM$_1$ from the UWFPS study could have been from traffic emissions and was highest in the Salt Lake Valley as expected based on the higher urban density there. Note that this marker peak at *m/z* 57 could also be present in railroad and aircraft emissions.

Previous ground-based observations in this region indicate significant spatial and temporal variability in the contribution of residential wood combustion (Cropper et al., 2018; Mouteva et al., 2017; Baasandorj et al., 2017b). The data reported here indicate that organic material from wood combustion is not the dominant mass fraction on a regional scale. However, smoke ~~concentrations~~ emissions could contribute to most of the aerosol mass at smaller scales or in near source regions (Kelly et al., 2013).

Wood combustion may also have an indirect effect on the formation of inorganic aerosol via secondary pathways involving oxidation of VOCs emitted from this source. Other tracers of various organic aerosol emissions and secondary formation (e.g., black carbon, carbon monoxide) were not obtained from the aircraft during this project, making it difficult to determine the most important organic aerosol sources for the region.

3.4 Vertical profiles

Vertical profiles show that the aerosol volume and mass concentration was variable as function of height. Within 1 km above ground level (AGL) we observed in several individual vertical profiles, layers of aerosols at different heights in each location, at different times of the day at different evolutionary stages of the pollution episodes (Figure S7). These changes in aerosol concentrations as function of height were measured by both the UHSAS and the AMS (Figure 7). The possible causes for these layers could be related to a difference in sources, losses, or to the many transport and mixing mechanisms that occur in complex terrain as discussed in Hoch et al. (in preparation), that are difficult to constrain with our limited vertical measurements during the study (Baasandorj et al., 2018).

Figure 8 shows the average vertical profiles of NR-PM_1 and ammonium nitrate mass fraction for Cache Valley, Salt Lake Valley and Utah valley during Episode#2. On average, Cache and Salt Lake Valley showed either a constant or a slight~~ly~~ increase in aerosol mass with altitude, up to about 200 m AGL in Cache and up to about 400 m AGL in Salt Lake Valley. Utah Valley show a general decrease in aerosol mass with altitude, shallower in the first 300 m AGL and steeper between 300 and 450 m AGL. Cache and Salt Lake Valley also show a decrease in aerosol mass with altitude from 200 to 450 m AGL and from 400 to 700 m AGL respectively. The average vertical profiles of all the three valleys show a very clear transition where the aerosol mass is very low above 500 m AGL in Cache Valley, 700 m AGL in Salt Lake Valley and 650 m AGL in Utah Valley. The average vertical profiles of the ammonium mass fraction show for all the three valleys that 75% or more of the aerosol mass is ammonium nitrate and that this is true for the first 300 m AGL in Cache Valley, 500 m AGL in Salt Lake Valley and 300 m AGL in Utah Valley. Above those heights, the variability in the chemical composition of the aerosol particles increases and the ammonium nitrate fraction decreases. The marked difference aloft, where the aerosol mass is very low is also characterized by a fraction of ammonium nitrate of 50% or less, similar in composition to what we observed at lower altitudes in clean conditions.

Interestingly, in some vertical profiles (Figure S7), especially at intermediate mass loadings (from 2 to 17 $\mu g\ m^{-3}$), higher mass loadings correspond to larger ammonium nitrate mass fractions (Figure S7 c, e, n, o). However, in other vertical profiles, changes in mass loadings do not correspond to a change in chemical composition (Figure S7 d, j, l, m). The detection of larger fractions of ammonium nitrate at higher altitudes (Figure S7 f, n, o) might indicate formation of nitrate aloft. A clear change in chemical composition is always detectable between 500 and 1000 m AGL for all the locations. This change is related to the transition from the boundary layer, affected by regional sources, to the free troposphere affected by long-range transport, and consists of a clear change from ammonium nitrate dominated aerosol to sulfate and organic dominated aerosol, concomitant with a decrease in aerosol concentration.

3.5 Limiting Reagent of ammonium nitrate formation

A straightforward method of determining which gas phase precursor (ammonia or nitric acid) is the limiting reagent in ammonium nitrate aerosol formation for the region is to compare the ratios of each species in the gas phase to the total: e.g., ammonia divided by total ammonium NH_3/(NH_3 + NH_4^+) and nitric acid divided by total nitrate HNO_3/(HNO_3 + NO_3^-). Figure 9 shows these ratios for Cache, Salt Lake and Utah valleys and Figure S8 for the other areas of the study. For all three valleys, the nitric acid gas phase fraction is nearly always smaller than the gas phase fraction of ammonia. Because a stoichiometric, 1:1, ratio of nitric acid to ammonia is needed to form ammonium nitrate, nitric acid is clearly limiting the formation of ammonium nitrate. The fraction of gas phase nitric acid also tends to decrease sharply with increasing total mass concentrations, indicating that the available nitric acid partitions efficiently to the aerosol phase at relatively moderate aerosol mass concentrations. In contrast, the fraction of gas phase ammonia is larger, irrespective of particle mass concentration and decreases less steeply with increasing mass loadings (Figure 9).

The relative importance of nitric acid in controlling the total aerosol mass varies between the three valleys. For the Cache Valley, the gas phase fraction of nitric acid is always near zero due to relatively large amounts of total ammonium. The gas phase fraction of nitric acid in the Utah Valley is frequently near zero, indicating that slightly more nitric acid (or less ammonia) is available there compared to the Cache Valley. In contrast, the gas phase fraction of ammonia for the Salt Lake Valley is more frequently smaller than in Cache and Utah Valley, especially at the largest total aerosol mass concentrations. Thus, during the most polluted conditions in the Salt Lake Valley, gas phase ammonia is relatively less abundant, indicating a possible transition from nitric-acid-limited towards ammonia-limited ammonium nitrate formation as pollution episodes evolve.

4 Thermodynamic modeling of ammonium nitrate

A comparison between the measurements and the ISORROPIA model was carried out to investigate how effectively the measured partitioning between the aerosol and gas phases are represented by the thermodynamic model. We found that gas phase ammonia, gas phase hydrochloric acid, aerosol ammonium, and aerosol nitrate agree well with the model predictions (r^2 = 0.984, 0.962, 0.984, 0.997 respectively) while gas phase nitric acid and aerosol chloride (as ammonium chloride) are not well represented by the model (r^2 = 0.555 and 0.161, respectively; Figure S9, Table S1). It is important to note, however, that these two species have relatively lower mass concentrations and therefore have larger uncertainties associated with them. For example, the median HNO_3 concentration for polluted events was 0.6 µg m^3, comparable to 3 times the detection limit of the HRToF-CIMS. Furthermore, the detection limit is typically determined in low particulate nitrate conditions. Therefore, in "polluted conditions" often less than 2% of particulate nitrate evaporating in the inlet system could explain the amount of gas-phase HNO_3 detected by the HRToF-CIMS. The modeled gas phase nitric acid was neither consistently higher nor lower than measured, with no clear dependency on temperature nor relative humidity. The aerosol chloride concentrations predicted by ISORROPIA were generally larger than measured. This overestimate of particle chloride by ISORROPIA has been also observed with other datasets (Haskins et al., 2018) and may affect the scenarios described below, especially for the effect of reducing total nitrate concentrations.

4.1 Simulated response to decreasing precursors

We carried out simulations of different scenarios using ISORROPIA (Figures 10, S10 S11 and S12). Figure 10 shows the simulated decrease in total aerosol mass for two cases: one in which the total nitrate was reduced by a factor of two while keeping the total ammonium constant (blue), and one in which the total ammonium was reduced by a factor of two while keeping the total nitrate constant (orange). Reduction in total nitrate led to approximately a proportional decrease in total inorganic aerosol concentrations during polluted conditions and across all locations. Conversely, a decrease in ammonium gave a more variable response. In some regions, a 50% decrease in total ammonium gave a decrease in aerosol mass of 50% or close to it, while in other regions there was no change. Cache Valley did not respond to a decrease in total ammonium. In fact, most of the orange points for the simulated mass lay on the 1:1 line, indicating no decrease in total aerosol mass compared to the mass at current conditions. On the contrary, there was a proportional decrease in aerosol mass when the total nitrate was decreased (blue points along to 1:2 line). These results confirm that in this valley, there was an excess of gas phase ammonia and the NH_4NO_3 formation chemistry is nitrate limited. The Salt Lake Valley responded to a reduction of either total nitrate or total ammonium (both blue and orange points are closer to the 1:2 line than the 1:1 line), suggesting that limiting either species could reduce aerosol formation. Despite the mass balance analysis showing excess reduced nitrogen, the thermodynamic model shows the total aerosol mass to be nearly proportionally sensitive to reductions in the either reagents. The Utah Valley, similarly to the Salt Lake Valley, showed a response for the reduction of total nitrate or total ammonium, except for mass loadings lower than 20 μg m^{-3} where a cluster of data points shows no response to the reduction of total ammonium. The area above the Great Salt Lake and Cache Valley were the least sensitive to the reduction of total ammonium while all other locations show varying responses for aerosol nitrate and chloride to the decrease in total ammonium. Interestingly, the aerosol chloride in the Salt Lake Valley and over the Great Salt Lake showed a slight increase for the decrease in total nitrate, pointing to a change in aerosol composition from ammonium nitrate to ammonium chloride. It is important to note that ISORROPIA generally over-predicts aerosol chloride (see Figure S9) and decreases in total nitrate would potentially decrease the available total chloride from acid displacement reactions on the alkaline salts. Hence, the simulated total reduction of nitrate carries a larger uncertainty.

A comprehensive view of the sensitivity of total aerosol mass to reductions in total ammonium and nitrate is shown in Figure 11a. This sensitivity study is based on 100 ISORROPIA simulations where data for the entire region (the whole dataset) were used as the input; the total nitrate and/or the total ammonium were decreased at steps of 10% and for each step the average total aerosol mass was calculated from the model output. For example, the 20% contour line (~~orange~~yellow) shows the interpolation of the model output that leads to a 20% reduction in total mass. This plot suggests that while reductions in both total ammonium and total nitrate would be effective overall, the most effective strategy to reduce the total aerosol mass in the region is through reduction of the total nitrate. The orange 10% contour line is reached with total nitrate reductions of about 15% without total ammonium reductions (bottom axis) whereas the total ammonium reduction would have to be more than 20% to reach this contour line without total nitrate reductions (left axis). However, both reagents must decrease in order to achieve a reduction of total aerosol mass larger than ~~40~~60% relative to observed conditions. The importance of ammonium, once the total aerosol mass has been decreased, is shown as one-dimensional plots in Figure 11b and 11c where it is shown the simulated decrease in total aerosol mass by decreasing only total nitrate or only total ammonium.

Note that these predictions are somewhat simplified since the model includes total chloride ($HCl+Cl^-$) where the aerosol chloride is ammonium chloride and changes in the amount of either total ammonium or total nitrate can cause additional effects for ammonium chloride partitioning. Furthermore, the model tends to over-predict the amount of aerosol ammonium chloride compared to observations. In the real environment, decreases in total nitrate would likely cause decreases in available total chloride because less displacement of chloride by nitric acid should occur from refractory salts such as sodium, calcium, or magnesium chlorides.

5 Conclusions

During the Utah Winter Fine Particulate Study (UWFPS), we measured gas precursors and aerosols from a NOAA Twin Otter aircraft over Salt Lake City and the surrounding valleys from January 16th to February 12th, 2017. The NR-PM~~$_{2.5}$~~$_{1}$ mass loadings for the region varied from below the AMS detection limit of 0.38 to 72.4 µg m^{-3} (2nd and 98th percentiles). The most severe pollution episodes occurred during persistent cold air pool (PCAP) periods, when emissions were trapped near the surface in the three valleys studied (Salt Lake, Cache, and Utah). Aircraft measurements provide spatial and temporal evolution of the non-refractory aerosol chemical composition, as well as the aerosol spatial and temporal evolution.

The particle chemical composition during polluted conditions (aerosol mass > 17.5 µg m^{-3}) was markedly different compared to clean conditions (aerosol mass ≤ 2 µg m^{-3}). The aerosols during polluted conditions were characterized by large fractions of ammonium nitrate (74±5%) while the fractions of organic, sulfate (mostly ammonium sulfate) and chloride (in the form of ammonium chloride) were smaller (18±3%%, 6±3% and 2±2% respectively). This composition was uniform across all three valleys. The relatively low fraction of organic material indicated that wood combustion played a minor role in the direct formation of secondary aerosols during polluted conditions, as the amounts of the traditional biomass burning marker for the AMS spectra (f_{60}) were similar to the ones measured in locations where biomass burning is negligible. However, we cannot completely exclude the role of wood combustion in the regional aerosol mass concentrations as aging in the atmosphere can cause the AMS markers to appear similar to background levels and measurements of other biomass burning tracers such as acetonitrile and black carbon were not available to constrain the AMS observations. During clean conditions, the organic fraction dominated the mass of the aerosols (50±13%), ammonium nitrate still remained the second most abundant species (31±9%) followed by sulfate and chloride (13±7% and 6±6% respectively).

Vertical profiles of the polluted region often showed varying layers of aerosol concentrations alternating. These variations did not always correspond to marked changes in chemical composition, although sometimes we observed a larger ammonium nitrate aerosol mass fraction below the top of the cold air pool. Whether this observation is due to meteorology or chemistry remains unclear. Above the cold air pool, the aerosol mass concentrations dropped considerably and the composition was characteristic of free tropospheric aerosols from long-range transport with relatively more sulfate and organic material and less ammonium nitrate.

Using gas phase measurements of nitric acid and ammonia, we calculated the fraction of each species in the gas phase relative to the total (gas + aerosol). For all three valleys, the fraction of nitric acid in the gas phase was smaller than the gas phase fraction of ammonia, indicating that the formation of ammonium nitrate in the aerosol phase was limited by the amount of nitric acid in the gas phase. The relative importance of nitric acid in controlling aerosol mass was largest for the Cache Valley, intermediate for the Utah Valley, and less important for the Salt Lake Valley. The gas phase fraction of ammonia in the Salt Lake Valley is often less than one at the largest total aerosol mass concentrations, indicating that gas phase nitric acid potentially becomes less limiting as pollution episodes evolve under PCAP conditions.

The largest aerosol mass concentrations of ammonium nitrate occurred at temperatures below the ice frost point. The comparison between measurements and the output of ISORROPIA showed agreement for ammonia, hydrochloric acid, aerosol ammonium, and aerosol nitrate. Measured nitric acid and the observed total chloride partitioning is not well represented by the model, with aerosol ammonium chloride consistently larger in the model. However, for these species the uncertainties in the model are larger than the other chemical species because their measured ambient concentrations were much smaller.

When we simulated a 50% decrease in total (gas + aerosol) ammonium using ISORROPIA we found that Cache Valley did not show a decrease in total aerosol mass compared to measured total ammonium levels, while Salt Lake and Utah valleys showed a decrease of 44% and 37% respectively. When a 50% decrease in total nitrate was simulated, a 44% decrease in total aerosol mass was observed in all the three valleys, indicating that in all the locations NH_4NO_3 formation is controlled by nitric acid availability. However, with the evolution of the pollution episode under PCAP conditions over time, ammonium nitrate formation in the system appeared to become less nitric acid limited for Salt Lake Valley and Utah Valley, while Cache Valley always had excess ammonia.

Acknowledgments

The authors would like to acknowledge Utah Division of Air Quality for their support and collaboration during the study. We thank the NOAA Aircraft Operations Center for their dedication and professionalism, particularly the pilots Robert Mitchel and Jason Clark for skillful navigation in complex terrain and challenging meteorology. We thank Frank Erdesz for helping with the installation of the UHSAS, Kyle Zarzana for helping with the calibration and installation of the NOxCARD, Patrick Veres for helping with the calibration of the HRToF-CIMS. We thank Tim Morphy and Teledyne for the loan of the $PM_{2.5}$ monitor at the Logan site. We thank Jon Abbatt at the University of Toronto and with the Canadian Aerosol Research Network, funded by the Canada Foundation for Innovation, for lending the UHSAS.

References

Aiken, A. C., DeCarlo, P. F., and Jimenez, J. L.: Elemental analysis of organic species with electron ionization high-resolution mass spectrometry, Analytical chemistry, 79, 8350-8358, 10.1021/ac071150w, 2007.

Aiken, A. C., Decarlo, P. F., Kroll, J. H., Worsnop, D. R., Huffman, J. A., Docherty, K. S., Ulbrich, I. M., Mohr, C., Kimmel, J. R., Sueper, D., Sun, Y., Zhang, Q., Trimborn, A., Northway, M., Ziemann, P. J., Canagaratna, M. R., Onasch, T. B., Alfarra, M. R., Prevot, A. S. H., Dommen, J., Duplissy, J., Metzger, A., Baltensperger, U., and Jimenez, J. L.: O/C and OM/OC ratios of primary, secondary, and ambient organic aerosols with high-resolution time-of-flight aerosol mass spectrometry, Environmental science & technology, 42, 4478-4485, 10.1021/es703009q, 2008.

Alfarra, M. R., Prevot, A. S. H., Szidat, S., Sandradewi, J., Weimer, S., Lanz, V. A., Schreiber, D., Mohr, M., and Baltensperger, U.: Identification of the mass spectral signature of organic aerosols from wood burning emissions, Environmental science & technology, 41, 5770-5777, 10.1021/es062289b, 2007.

Allan, J. D., Delia, A. E., Coe, H., Bower, K. N., Alfarra, M. R., Jimenez, J. L., Middlebrook, A. M., Drewnick, F., Onasch, T. B., Canagaratna, M. R., Jayne, J. T., and Worsnop, D. R.: A generalised method for the extraction of chemically resolved mass spectra from aerodyne aerosol mass spectrometer data, J Aerosol Sci, 35, 909-922, 10.1016/j.jaerosci.2004.02.007, 2004.

Baasandorj, M., Hoch, S. W., Bares, R., Lin, J. C., Brown, S. S., Millet, D. B., Martin, R., Kelly, K., Zarzana, K. J., Whiteman, C. D., Dube, W. P., Tonnesen, G., Jaramillo, I. C., and Sohl, J.: Coupling between Chemical and Meteorological Processes under Persistent Cold-Air Pool Conditions: Evolution of Wintertime PM2.5 Pollution Events and N2O5 Observations in Utah's Salt Lake Valley, Environmental science & technology, 51, 5941-5950, 10.1021/acs.est.6b06603, 2017.

Baasandorj, M., D.J. Eatough, P.M. Cropper, D.K. Overson, J.C. Hansen, R. Kuprov, and J.H. Lin, West Valley City High Time Resolution Air Toxics Study Report, 2017. https://documents.deq.utah.gov/air-quality/planning/technical-analysis/research/air-toxics/WVC/DAQ-2017-017121.pdf (Last accessed: June 2018).

Baasandorj, M., Brown, S. S., Hoch, S., Crosman, E., Long R., Silva, P. Mitchell L., Hammond I., Martin, R., Bares R., Lin, J., Sohl J.,Page, J., McKeen, S., Pennell, C., Franchin, A., Middlebrook, A., Petersen, R., Hallar, G., Fibiger, D., Womack, C., McDuffie, E., Moravek, A., Murphy, J., Hrdina, A., Thornton, J., Goldberger, L., Lee, B., Riedel, T., Whitehill, A., Kelly, K., Hansen, J., Eatough, D., 2017 Utah Winter Fine Particulate Study Final Report, 2017.https://www.esrl.noaa.gov/csd/groups/csd7/measurements/2017uwfps/finalreport.pdf (Last accessed June 2018)

Bahreini, R., Dunlea, E. J., Matthew, B. M., Simons, C., Docherty, K. S., DeCarlo, P. F., Jimenez, J. L., Brock, C. A., and Middlebrook, A. M.: Design and operation of a pressure-controlled inlet for airborne sampling with an aerodynamic aerosol lens, Aerosol Sci Tech, 42, 465-471, 10.1080/02786820802178514, 2008.

Bahreini, R., Ervens, B., Middlebrook, A. M., Warneke, C., de Gouw, J. A., DeCarlo, P. F., Jimenez, J. L., Brock, C. A., Neuman, J. A., Ryerson, T. B., Stark, H., Atlas, E., Brioude, J., Fried, A., Holloway, J. S., Peischl, J., Richter, D., Walega, J., Weibring, P., Wollny, A. G., and Fehsenfeld, F. C.: Organic aerosol formation in urban and industrial plumes near Houston and Dallas, Texas, J Geophys Res-Atmos, 114, Artn D00f16 10.1029/2008jd011493, 2009.

Beard, J. D., Beck, C., Graham, R., Packham, S. C., Traphagan, M., Giles, R. T., and Morgan, J. G.: Winter Temperature Inversions and Emergency Department Visits for Asthma in Salt Lake County, Utah, 2003-2008, Environ Health Persp, 120, 1385-1390, 10.1289/ehp.1104349, 2012.

Bessagnet, B., Hodzic, A., Blanchard, O., Lattuati, M., Le Bihan, O., Marfaing, H., and Rouil, L.: Origin of particulate matter pollution episodes in wintertime over the Paris Basin, Atmos Environ, 39, 6159-6174, 10.1016/j.atmosenv.2005.06.053, 2005.

Bondy, A. L., Wang, B. B., Laskin, A., Craig, R. L., Nhliziyo, M. V., Bertman, S. B., Pratt, K. A., Shepson, P. B., and Ault, A. P.: Inland Sea Spray Aerosol Transport and Incomplete Chloride Depletion: Varying Degrees of Reactive Processing Observed during SOAS, Environmental science & technology, 51, 9533-9542, 10.1021/acs.est.7b02085, 2017.

Brock, C. A., Cozic, J., Bahreini, R., Froyd, K. D., Middlebrook, A. M., McComiskey, A., Brioude, J., Cooper, O. R., Stohl, A., Aikin, K. C., de Gouw, J. A., Fahey, D. W., Ferrare, R. A., Gao, R. S., Gore, W., Holloway, J. S., Hubler, G., Jefferson, A., Lack, D. A., Lance, S., Moore, R. H., Murphy, D. M., Nenes, A., Novelli, P. C., Nowak, J. B., Ogren, J. A., Peischl, J., Pierce, R. B., Pilewskie, P., Quinn, P. K., Ryerson, T. B., Schmidt, K. S., Schwarz, J. P., Sodemann, H., Spackman, J. R., Stark, H., Thomson, D. S., Thornberry, T., Veres, P., Watts, L. A., Warneke, C., and Wollny, A. G.: Characteristics, sources, and transport of aerosols measured in spring 2008 during the aerosol, radiation, and cloud processes affecting Arctic Climate (ARCPAC) Project, Atmos Chem Phys, 11, 2423-2453, 10.5194/acp-11-2423-2011, 2011.

Brown, S. G., Roberts, P. T., McCarthy, M. C., Lurmann, F. W., and Hyslop, N. P.: Wintertime vertical variations in particulate matter (PM) and precursor concentrations in the San Joaquin Valley during the California Regional coarse PM/fine

PM Air Quality Study, Journal of the Air & Waste Management Association, 56, 1267-1277, Doi 10.1080/10473289.2006.10464583, 2006.

Brown, S. S., Thornton, J. A., Keene, W. C., Pszenny, A. A. P., Sive, B. C., Dube, W. P., Wagner, N. L., Young, C. J., Riedel, T. P., Roberts, J. M., VandenBoer, T. C., Bahreini, R., Ozturk, F., Middlebrook, A. M., Kim, S., Hubler, G., and Wolfe, D. E.: Nitrogen, Aerosol Composition, and Halogens on a Tall Tower (NACHTT): Overview of a wintertime air chemistry field study in the front range urban corridor of Colorado, J Geophys Res-Atmos, 118, 8067-8085, 10.1002/jgrd.50537, 2013.

Cai, Y., Montague, D. C., Mooiweer-Bryan, W., and Deshler, T.: Performance characteristics of the ultra high sensitivity aerosol spectrometer for particles between 55 and 800 nm: Laboratory and field studies, J Aerosol Sci, 39, 759-769, 10.1016/j.jaerosci.2008.04.007, 2008.

Canagaratna, M. R., Jayne, J. T., Ghertner, D. A., Herndon, S., Shi, Q., Jimenez, J. L., Silva, P. J., Williams, P., Lanni, T., Drewnick, F., Demerjian, K. L., Kolb, C. E., and Worsnop, D. R.: Chase studies of particulate emissions from in-use New York City vehicles, Aerosol Sci Tech, 38, 555-573, 10.1080/02786820490465504, 2004.

Canagaratna, M. R., Jayne, J. T., Jimenez, J. L., Allan, J. D., Alfarra, M. R., Zhang, Q., Onasch, T. B., Drewnick, F., Coe, H., Middlebrook, A., Delia, A., Williams, L. R., Trimborn, A. M., Northway, M. J., DeCarlo, P. F., Kolb, C. E., Davidovits, P., and Worsnop, D. R.: Chemical and microphysical characterization of ambient aerosols with the aerodyne aerosol mass spectrometer, Mass Spectrom Rev, 26, 185-222, 10.1002/mas.20115, 2007.

Canagaratna, M. R., Jimenez, J. L., Kroll, J. H., Chen, Q., Kessler, S. H., Massoli, P., Hildebrandt Ruiz, L., Fortner, E., Williams, L. R., Wilson, K. R., Surratt, J. D., Donahue, N. M., Jayne, J. T., and Worsnop, D. R.: Elemental ratio measurements of organic compounds using aerosol mass spectrometry: characterization, improved calibration, and implications, Atmos Chem Phys, 15, 253-272, 10.5194/acp-15-253-2015, 2015.

Chen, L. W. A., Watson, J. G., Chow, J. C., Green, M. C., Inouye, D., and Dick, K.: Wintertime particulate pollution episodes in an urban valley of the Western US: a case study, Atmos Chem Phys, 12, 10051-10064, 10.5194/acp-12-10051-2012, 2012.

Chow, J. C., Chen, L. W. A., Watson, J. G., Lowenthal, D. H., Magliano, K. A., Turkiewicz, K., and Lehrman, D. E.: PM2.5 chemical composition and spatiotemporal variability during the California Regional PM10/PM2.5 Air Quality Study (CRPAQS), J Geophys Res-Atmos, 111, Artn D10s04 10.1029/2005jd006457, 2006.

Corbin, J. C., Keller, A., Lohmann, U., Burtscher, H., Sierau, B., and Mensah, A. A.: Organic Emissions from a Wood Stove and a Pellet Stove Before and After Simulated Atmospheric Aging, Aerosol Sci Tech, 49, 1037-1050, 10.1080/02786826.2015.1079586, 2015.

Cropper, P. M., Eatough, D. J., Overson, D. K., Hansen, J. C., Caka, F., and Cary, R. A.: Use of a gas chromatography-mass spectrometry organic aerosol monitor for in-field detection of fine particulate organic compounds in source apportionment, Journal of the Air & Waste Management Association, 68, 390-402, 10.1080/10962247.2017.1363095, 2018.

Cubison, M. J., Ortega, A. M., Hayes, P. L., Farmer, D. K., Day, D., Lechner, M. J., Brune, W. H., Apel, E., Diskin, G. S., Fisher, J. A., Fuelberg, H. E., Hecobian, A., Knapp, D. J., Mikoviny, T., Riemer, D., Sachse, G. W., Sessions, W., Weber, R. J., Weinheimer, A. J., Wisthaler, A., and Jimenez, J. L.: Effects of aging on organic aerosol from open biomass burning smoke in aircraft and laboratory studies, Atmos Chem Phys, 11, 12049-12064, 10.5194/acp-11-12049-2011, 2011.

Drewnick, F., Hings, S. S., DeCarlo, P., Jayne, J. T., Gonin, M., Fuhrer, K., Weimer, S., Jimenez, J. L., Demerjian, K. L., Borrmann, S., and Worsnop, D. R.: A new time-of-flight aerosol mass spectrometer (TOF-AMS) - Instrument description and first field deployment, Aerosol Sci Tech, 39, 637-658, 10.1080/02786820500182040, 2005.

Ellis, R. A., Murphy, J. G., Pattey, E., van Haarlem, R., O'Brien, J. M., and Herndon, S. C.: Characterizing a Quantum Cascade Tunable Infrared Laser Differential Absorption Spectrometer (QC-TILDAS) for measurements of atmospheric ammonia, Atmos Meas Tech, 3, 397-406, DOI 10.5194/amt-3-397-2010, 2010.

Elsasser, M., Crippa, M., Orasche, J., DeCarlo, P. F., Oster, M., Pitz, M., Cyrys, J., Gustafson, T. L., Pettersson, J. B. C., Schnelle-Kreis, J., Prevot, A. S. H., and Zimmermann, R.: Organic molecular markers and signature from wood combustion particles in winter ambient aerosols: aerosol mass spectrometer (AMS) and high time-resolved GC-MS measurements in Augsburg, Germany, Atmos Chem Phys, 12, 6113-6128, 10.5194/acp-12-6113-2012, 2012.

Favez, O., El Haddad, I., Piot, C., Boreave, A., Abidi, E., Marchand, N., Jaffrezo, J. L., Besombes, J. L., Personnaz, M. B., Sciare, J., Wortham, H., George, C., and D'Anna, B.: Inter-comparison of source apportionment models for the estimation of wood burning aerosols during wintertime in an Alpine city (Grenoble, France), Atmos Chem Phys, 10, 5295-5314, 10.5194/acp-10-5295-2010, 2010.

Fountoukis, C., and Nenes, A.: ISORROPIA II: a computationally efficient thermodynamic equilibrium model for K+-Ca2+-Mg2+-Nh(4)(+)-Na+-SO42--NO3--Cl--H2O aerosols, Atmos Chem Phys, 7, 4639-4659, DOI 10.5194/acp-7-4639-2007, 2007.

Fuchs, H., Dube, W. P., Lerner, B. M., Wagner, N. L., Williams, E. J., and Brown, S. S.: A Sensitive and Versatile Detector for Atmospheric NO2 and NOx Based on Blue Diode Laser Cavity Ring-Down Spectroscopy, Environmental science & technology, 43, 7831-7836, 10.1021/es902067h, 2009.

Green, M. C., Chow, J. C., Watson, J. G., Dick, K., and Inouye, D.: Effects of Snow Cover and Atmospheric Stability on Winter PM2.5 Concentrations in Western U.S. Valleys, J Appl Meteorol Clim, 54, 1191-1201, 10.1175/Jamc-D-14-0191.1, 2015.

Gwaze, P., Helas, G., Annegarn, H. J., Huth, J., and Piketh, S. J.: Physical, chemical and optical properties of aerosol particles collected over Cape Town during winter haze episodes, S Afr J Sci, 103, 35-43, 2007.

Hansen, J. C., Woolwine, W. R., Bates, B. L., Clark, J. M., Kuprov, R. Y., Mukherjee, P., Murray, J. A., Simmons, M. A., Waite, M. F., Eatough, N. L., Eatough, D. J., Long, R., and Grover, B. D.: Semicontinuous PM2.5 and PM10 Mass and Composition Measurements in Lindon, Utah, during Winter 2007, Journal of the Air & Waste Management Association, 60, 346-355, 10.3155/1047-3289.60.3.346, 2010.

Haskins et al, JGR 2018 submitted (under review)

Heringa, M. F., DeCarlo, P. F., Chirico, R., Lauber, A., Doberer, A., Good, J., Nussbaumer, T., Keller, A., Burtscher, H., Richard, A., Miljevic, B., Prevot, A. S. H., and Baltensperger, U.: Time-Resolved Characterization of Primary Emissions from Residential Wood Combustion Appliances, Environmental science & technology, 46, 11418-11425, 10.1021/es301654w, 2012.

Hoch et al. (in preparation)

Jayne, J. T., Leard, D. C., Zhang, X. F., Davidovits, P., Smith, K. A., Kolb, C. E., and Worsnop, D. R.: Development of an aerosol mass spectrometer for size and composition analysis of submicron particles, Aerosol Sci Tech, 33, 49-70, Doi 10.1080/027868200410840, 2000.

Junninen, H., Ehn, M., Petaja, T., Luosujarvi, L., Kotiaho, T., Kostiainen, R., Rohner, U., Gonin, M., Fuhrer, K., Kulmala, M., and Worsnop, D. R.: A high-resolution mass spectrometer to measure atmospheric ion composition, Atmos Meas Tech, 3, 1039-1053, 10.5194/amt-3-1039-2010, 2010.

Kelly, K. E., Kotchenruther, R., Kuprov, R., and Silcox, G. D.: Receptor model source attributions for Utah's Salt Lake City airshed and the impacts of wintertime secondary ammonium nitrate and ammonium chloride aerosol, Journal of the Air & Waste Management Association, 63, 575-590, 10.1080/10962247.2013.774819, 2013.

Kim, Y. J., Spak, S. N., Carmichael, G. R., Riemer, N., and Stanier, C. O.: Modeled aerosol nitrate formation pathways during wintertime in the Great Lakes region of North America, J Geophys Res-Atmos, 119, 12420-12445, 10.1002/2014JD022320, 2014.

Kleindienst, T. E., Lewandowski, M., Offenberg, J. H., Edney, E. O., Jaoui, M., Zheng, M., Ding, X. A., and Edgerton, E. S.: Contribution of Primary and Secondary Sources to Organic Aerosol and PM2.5 at SEARCH Network Sites, Journal of the Air & Waste Management Association, 60, 1388-1399, 10.3155/1047-3289.60.11.1388, 2010.

Kotchenruther, R. A.: Source apportionment of PM2.5 at multiple Northwest US sites: Assessing regional winter wood smoke impacts from residential wood combustion, Atmos Environ, 142, 210-219, 10.1016/j.atmosenv.2016.07.048, 2016.

Kuprov, R., Eatough, D. J., Cruickshank, T., Olson, N., Cropper, P. M., and Hansen, J. C.: Composition and secondary formation of fine particulate matter in the Salt Lake Valley: Winter 2009, Journal of the Air & Waste Management Association, 64, 957-969, 10.1080/10962247.2014.903878, 2014.

Lareau, N. P., Crosman, E., Whiteman, C. D., Horel, J. D., Hoch, S. W., Brown, W. O. J., and Horst, T. W.: The Persistent Cold-Air Pool Study, B Am Meteorol Soc, 94, 51-63, 10.1175/Bams-D-11-00255.1, 2013.

Lee, B. H., Lopez-Hilfiker, F. D., Mohr, C., Kurten, T., Worsnop, D. R., and Thornton, J. A.: An Iodide-Adduct High-Resolution Time-of-Flight Chemical-Ionization Mass Spectrometer: Application to Atmospheric Inorganic and Organic Compounds, Environmental science & technology, 48, 6309-6317, 10.1021/es500362a, 2014.

Lee, B. H., Lopez-Hilfiker, F. D., Veres, P. R., McDuffie, E. E., Fibiger, D. L., Sparks, T. L., et al. (2018). Flight Deployment of a High-Resolution Time-of-Flight Chemical Ionization Mass Spectrometer: Observations of Reactive Halogen and Nitrogen Oxide Species. Journal of Geophysical Research: Atmospheres. https://doi.org/10.1029/2017JD028082

Liao, J., Brock, C. A., Murphy, D. M., Sueper, D. T., Welti, A., and Middlebrook, A. M.: Single-particle measurements of bouncing particles and in situ collection efficiency from an airborne aerosol mass spectrometer (AMS) with light-scattering detection, Atmos Meas Tech, 10, 3801-3820, 10.5194/amt-10-3801-2017, 2017.

Lurmann, F. W., Brown, S. G., McCarthy, M. C., and Roberts, P. T.: Processes influencing secondary aerosol formation in the San Joaquin Valley during winter, Journal of the Air & Waste Management Association, 56, 1679-1693, Doi 10.1080/10473289.2006.10464573, 2006.

Mangelson, N. F., Lewis, L., Joseph, J. M., Cui, W. X., Machir, J., Williams, N. W., Eatough, D. J., Rees, L. B., Wilkerson, T., and Jensen, D. T.: The contribution of sulfate and nitrate to atmospheric fine particles during winter inversion fogs in Cache Valley, Utah, Journal of the Air & Waste Management Association, 47, 167-175, Doi 10.1080/10473289.1997.10464429, 1997.

McDuffie, E. E., Fibiger, D. L., Dube, W. P., Lopez-Hilfiker, F., Lee, B. H., Thornton, J. A., Shah, V., Jaegle, L., Guo, H. Y., Weber, R. J., Reeves, J. M., Weinheimer, A. J., Schroder, J. C., Campuzano-Jost, P., Jimenez, J. L., Dibb, J. E., Veres, P., Ebben, C., Sparks, T. L., Wooldridge, P. J., Cohen, R. C., Hornbrook, R. S., Apel, E. C., Campos, T., Hall, S. R., Ullmann, K., and Brown, S. S.: Heterogeneous N2O5 Uptake During Winter: Aircraft Measurements During the 2015 WINTER Campaign and Critical Evaluation of Current Parameterizations, J Geophys Res-Atmos, 123, 4345-4372, 10.1002/2018JD028336, 2018.

Metzger, S., Mihalopoulos, N., and Lelieveld, J.: Importance of mineral cations and organics in gas-aerosol partitioning of reactive nitrogen compounds: case study based on MINOS results, Atmos Chem Phys, 6, 2549-2567, DOI 10.5194/acp-6-2549-2006, 2006.

Mouteva, G. O., Randerson, J. T., Fahrni, S. M., Bush, S. E., Ehleringer, J. R., Xu, X. M., Santos, G. M., Kuprov, R., Schichtel, B. A., and Czimczik, C. I.: Using radiocarbon to constrain black and organic carbon aerosol sources in Salt Lake City, J Geophys Res-Atmos, 122, 9843-9857, 10.1002/2017JD026519, 2017.

Nenes, A., Pandis, S. N., and Pilinis, C.: ISORROPIA: A new thermodynamic equilibrium model for multiphase multicomponent inorganic aerosols, Aquat Geochem, 4, 123-152, Doi 10.1023/A:1009604003981, 1998.

Ng, N. L., Canagaratna, M. R., Zhang, Q., Jimenez, J. L., Tian, J., Ulbrich, I. M., Kroll, J. H., Docherty, K. S., Chhabra, P. S., Bahreini, R., Murphy, S. M., Seinfeld, J. H., Hildebrandt, L., Donahue, N. M., DeCarlo, P. F., Lanz, V. A., Prevot, A. S. H., Dinar, E., Rudich, Y., and Worsnop, D. R.: Organic aerosol components observed in Northern Hemispheric datasets from Aerosol Mass Spectrometry, Atmos Chem Phys, 10, 4625-4641, 10.5194/acp-10-4625-2010, 2010.

Ortega, A. M., Day, D. A., Cubison, M. J., Brune, W. H., Bon, D., de Gouw, J. A., and Jimenez, J. L.: Secondary organic aerosol formation and primary organic aerosol oxidation from biomass-burning smoke in a flow reactor during FLAME-3, Atmos Chem Phys, 13, 11551-11571, 10.5194/acp-13-11551-2013, 2013.

Perring, A. E., Schwarz, J. P., Gao, R. S., Heymsfield, A. J., Schmitt, C. G., Schnaiter, M., and Fahey, D. W.: Evaluation of a Perpendicular Inlet for Airborne Sampling of Interstitial Submicron Black-Carbon Aerosol, Aerosol Sci Tech, 47, 1066-1072, 10.1080/02786826.2013.821196, 2013.

Petetin, H., Sciare, J., Bressi, M., Gros, V., Rosso, A., Sanchez, O., Sarda-Estève, R., Petit, J.-E., and Beekmann, M.: Assessing the ammonium nitrate formation regime in the Paris megacity and its representation in the CHIMERE model, Atmos. Chem. Phys., 16, 10419-10440, https://doi.org/10.5194/acp-16-10419-2016, 2016.

Pope, C. A., Muhlestein, J. B., May, H. T., Renlund, D. G., Anderson, J. L., and Horne, B. D.: Ischemic heart disease events triggered by short-term exposure to fine particulate air pollution, Circulation, 114, 2443-2448, 10.1161/Circulationaha.106.636977, 2006.

Prabhakar, G., Parworth, C. L., Zhang, X. L., Kim, H., Young, D. E., Beyersdorf, A. J., Ziemba, L. D., Nowak, J. B., Bertram, T. H., Faloona, I. C., Zhang, Q., and Cappa, C. D.: Observational assessment of the role of nocturnal residual-layer chemistry in determining daytime surface particulate nitrate concentrations, Atmos Chem Phys, 17, 14747-14770, 10.5194/acp-17-14747-2017, 2017.

Ricciardelli, I., Bacco, D., Rinaldi, M., Bonafe, G., Scotto, F., Trentini, A., Bertacci, G., Ugolini, P., Zigola, C., Rovere, F., Maccone, C., Pironi, C., and Poluzzi, V.: A three-year investigation of daily PM2.5 main chemical components in four sites: the routine measurement program of the Supersito Project (Po Valley, Italy), Atmos Environ, 152, 418-430, 10.1016/j.atmosenv.2016.12.052, 2017.

Schneider, J., Weimer, S., Drewnick, F., Borrmann, S., Helas, G., Gwaze, P., Schmid, O., Andreae, M. O., and Kirchner, U.: Mass spectrometric analysis and aerodynamic properties of various types of combustion-related aerosol particles, Int J Mass Spectrom, 258, 37-49, 10.1016/j.ijms.2006.07.008, 2006.

Shrivastava, M. K., Subramanian, R., Rogge, W. F., and Robinson, A. L.: Sources of organic aerosol: Positive matrix factorization of molecular marker data and comparison of results from different source apportionment models, Atmos Environ, 41, 9353-9369, 10.1016/j.atmosenv.2007.09.016, 2007.

Stanier, C., Singh, A., Adamski, W., Baek, J., Caughey, M., Carmichael, G., Edgerton, E., Kenski, D., Koerber, M., Oleson, J., Rohlf, T., Lee, S. R., Riemer, N., Shaw, S., Sousan, S., and Spak, S. N.: Overview of the LADCO winter nitrate study: hourly ammonia, nitric acid and PM2.5 composition at an urban and rural site pair during PM2.5 episodes in the US Great Lakes region, Atmos Chem Phys, 12, 11037-11056, 10.5194/acp-12-11037-2012, 2012.

Sudheer, A. K., and Rengarajan, R.: Time-resolved inorganic chemical composition of fine aerosol and associated precursor gases over an urban environment in western India: Gas-aerosol equilibrium characteristics, Atmos Environ, 109, 217-227, 10.1016/j.atmosenv.2015.03.028, 2015.

Tevlin, A. G., Li, Y., Collett, J. L., McDuffie, E. E., Fischer, E. V., and Murphy, J. G.: Tall Tower Vertical Profiles and Diurnal Trends of Ammonia in the Colorado Front Range, J Geophys Res-Atmos, 122, 12468-12487, 10.1002/2017JD026534, 2017.

Trebs, I., Metzger, S., Meixner, F. X., Helas, G. N., Hoffer, A., Rudich, Y., Falkovich, A. H., Moura, M. A. L., da Silva, R. S., Artaxo, P., Slanina, J., and Andreae, M. O.: The NH4+-NO3--Cl--SO42--H2O aerosol system and its gas phase precursors at a pasture site in the Amazon Basin: How relevant are mineral cations and soluble organic acids?, J Geophys Res-Atmos, 110, Artn D07303 10.1029/2004jd005478, 2005.

Wang, D. X., Hu, J. L., Xu, Y., Lv, D., Xie, X. Y., Kleeman, M., Xing, J., Zhang, H. L., and Ying, Q.: Source contributions to primary and secondary inorganic particulate matter during a severe wintertime PM2.5 pollution episode in Xi'an, China, Atmos Environ, 97, 182-194, 10.1016/j.atmosenv.2014.08.020, 2014.

Washenfelder, R. A., Wagner, N. L., Dube, W. P., and Brown, S. S.: Measurement of Atmospheric Ozone by Cavity Ring-down Spectroscopy, Environmental science & technology, 45, 2938-2944, 10.1021/es103340u, 2011.

Watson, J. G., and Chow, J. C.: A wintertime PM2.5 episode at the fresno, CA, supersite, Atmos Environ, 36, 465-475, Doi 10.1016/S1352-2310(01)00309-0, 2002.

Whiteman, C. D., Hoch, S. W., Horel, J. D., and Charland, A.: Relationship between particulate air pollution and meteorological variables in Utah's Salt Lake Valley, Atmos Environ, 94, 742-753, 10.1016/j.atmosenv.2014.06.012, 2014.

Wild, R. J., Edwards, P. M., Dube, W. P., Baumann, K., Edgerton, E. S., Quinn, P. K., Roberts, J. M., Rollins, A. W., Veres, P. R., Warneke, C., Williams, E. J., Yuan, B., and Brown, S. S.: A Measurement of Total Reactive Nitrogen, NOy, together with NO2, NO, and O-3 via Cavity Ring-down Spectroscopy, Environmental science & technology, 48, 9609-9615, 10.1021/es501896w, 2014.

Woody, M. C., Baker, K. R., Hayes, P. L., Jimenez, J. L., Koo, B., and Pye, H. O. T.: Understanding sources of organic aerosol during CalNex-2010 using the CMAQ-VBS, Atmos Chem Phys, 16, 4081-4100, DOI 10.5194/acp-16-4081-2016, 2016.

Zhang, Q., Alfarra, M. R., Worsnop, D. R., Allan, J. D., Coe, H., Canagaratna, M. R., and Jimenez, J. L.: Deconvolution and quantification of hydrocarbon-like and oxygenated organic aerosols based on aerosol mass spectrometry, Environmental science & technology, 39, 4938-4952, 10.1021/es048568l, 2005.

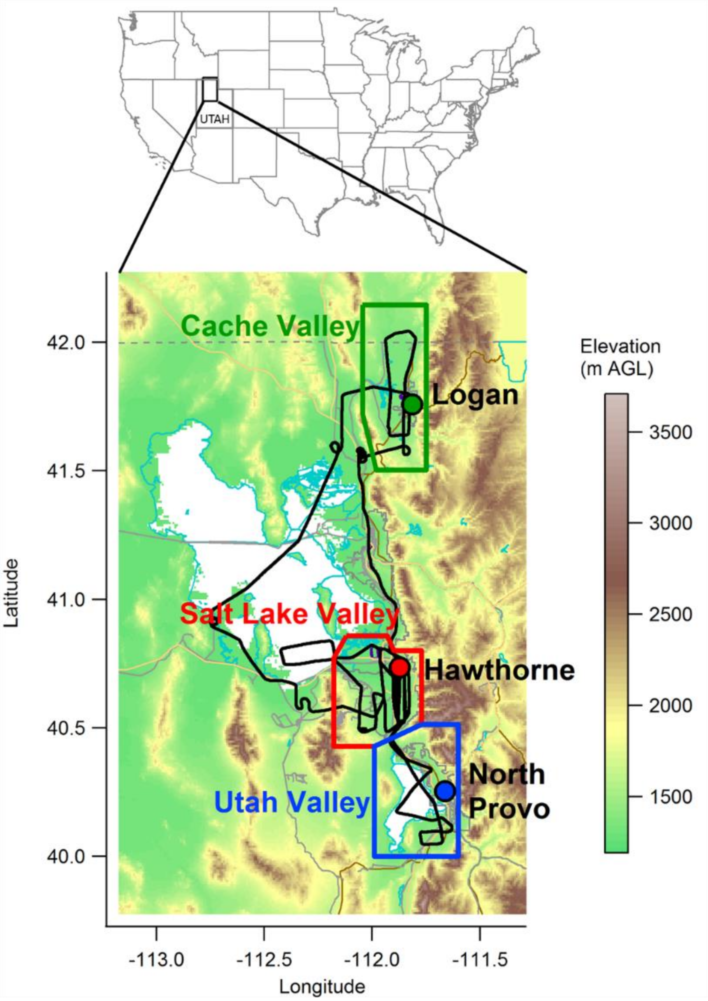

Figure 1: Map showing the area studied during the UWFPS. Top: map of the United States with the region of interest of this study highlighted by a black rectangle. Bottom: detail of the area of interest colored by elevation as shown in the color bar. In black is shown a typical flight track. The Cache Valley study region is outlined in green, Salt Lake Valley in red and Utah Valley in blue. The circles with the same color pattern and labeled in black represent the locations of the ground sites with data presented here.

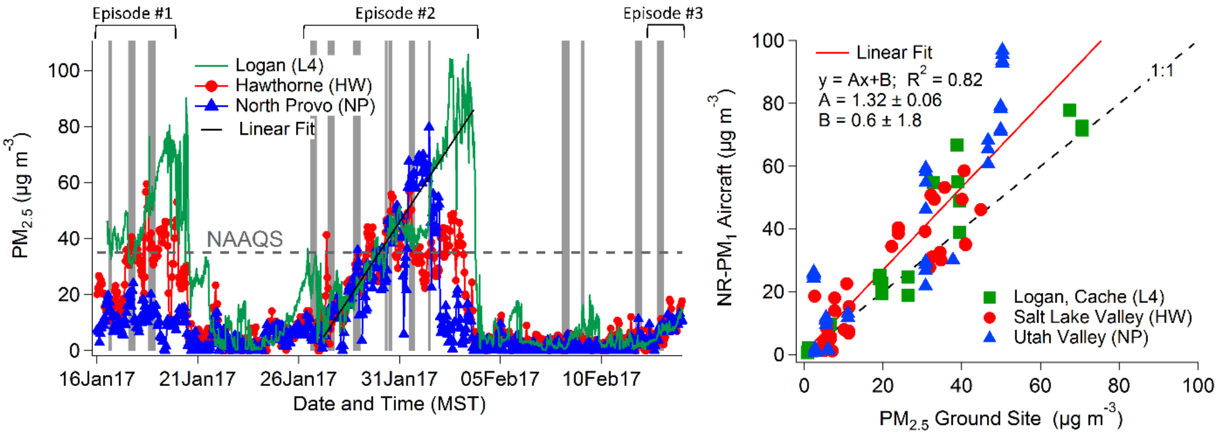

Figure 2: $PM_{2.5}$ measurements from three ground sites during UWFPS. Left: time series of $PM_{2.5}$ measured in Logan (L4), Cache Valley in green; at Hawthorne Elementary School (HW), Salt Lake Valley, in red; and in North Provo (NP), Utah Valley, in blue. The grey shaded areas correspond to the times of Twin Otter flights; the horizontal dashed line indicates the National Ambient Air Quality Standard (NAAQS) of 35 ug m^{-3} for 24-hr averaged $PM_{2.5}$. The black solid line is a fit over all the data of increase in $PM_{2.5}$ during Episode#2. The slope is 10.89 ± 0.08 µg m^{-3} day^{-1} (slope ± 95% CI). Right: comparison of the non-refractory (NR) PM_1 measured with the AMS from the Twin Otter for altitudes lower than 50 m AGL during the missed approaches at the airports closest to the ground site measurements. The dashed line is the 1:1 line and the red solid line is a linear fit; correlation coefficient, fit coefficients and their 95% CI are reported in the legend.

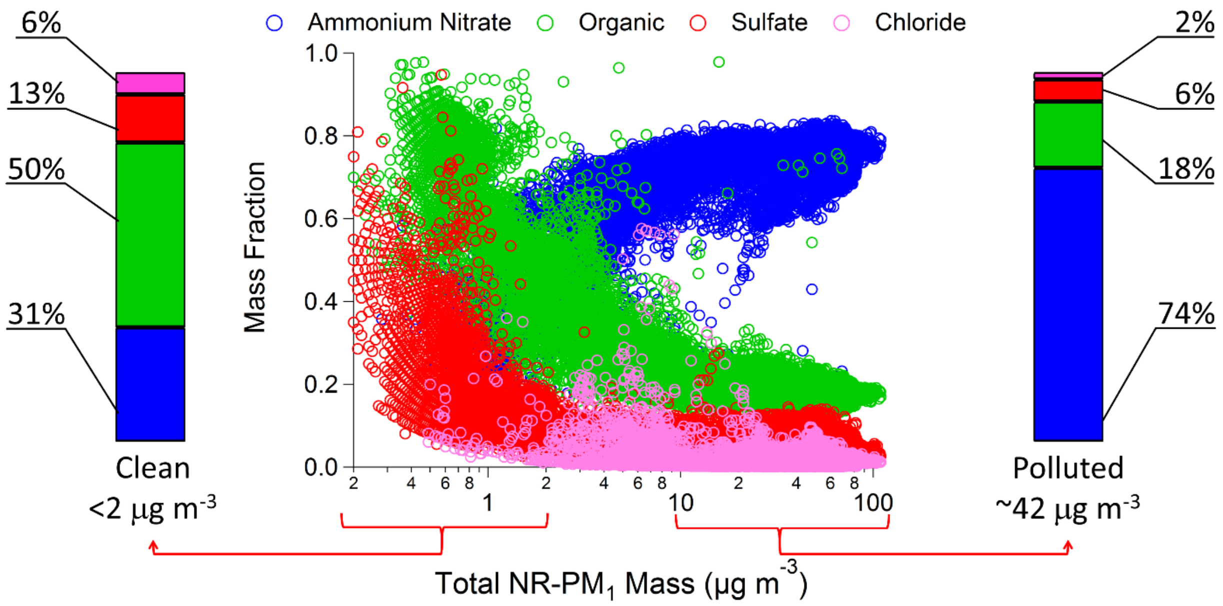

Figure 3: Center: Aerosol mass fraction as a function of the total mass of NR-PM$_1$ measured from the Twin Otter. Ammonium nitrate is in blue, organic in green, sulfate and chloride in red and pink, respectively. The bar chart on the left corresponds to the average of the mass fractions when the total aerosol mass is <2 µg sm^{-3} (clean conditions). The bar chart to the right corresponds to the average of the mass fractions when the total aerosol mass is >17.5 µg sm^{-3} (polluted conditions) and altitude is <900 m AGL (below the boundary layer).

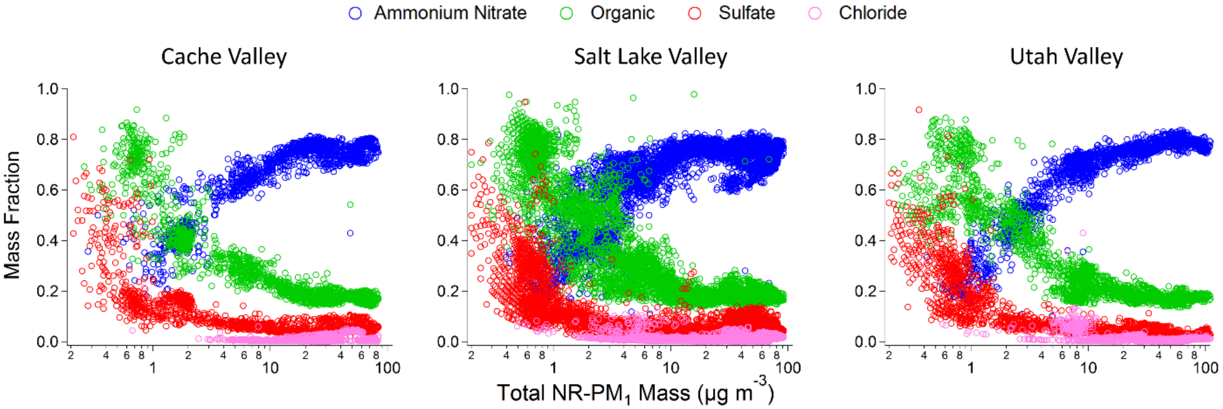

Figure 4: Aerosol mass fraction as a function of total NR-PM$_1$ mass for each of the three main study areas measured from the Twin Otter. Color-code same as Figure 3.

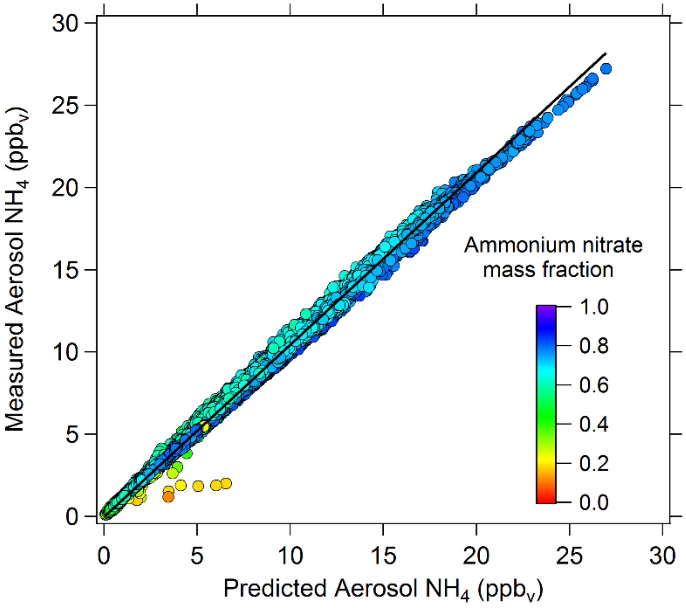

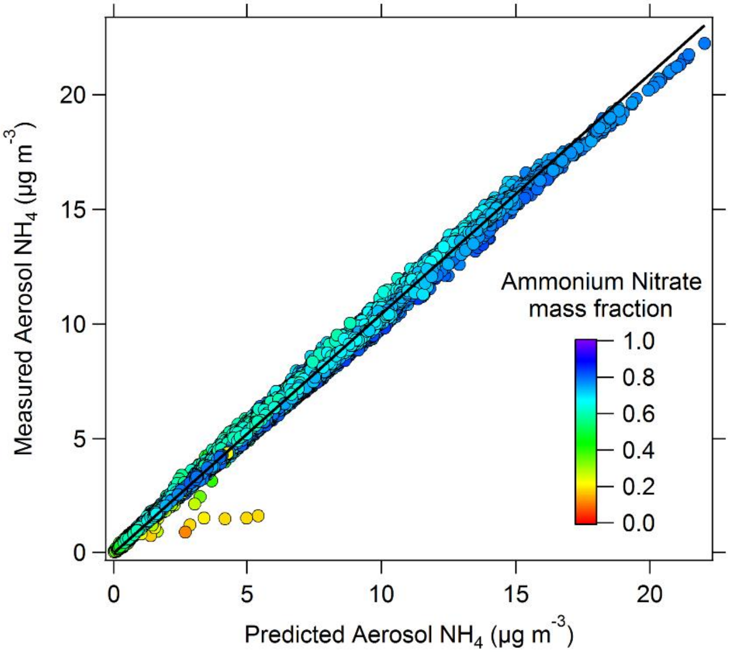

Figure 5: Aerosol ion balance from the AMS measurements. On the x-axis is the calculated mass of ammonium for fully neutralized aerosols (NH_4^+= 18*(NO_3^-/62 + SO_4^-/96*2 + Cl^-/35.45). On the y-axis is the measured ammonium (NH_4^+) in the aerosol particles. The black line is the 1:1 line, where points on the line correspond to neutralized aerosols and below the line are acidic aerosols. Data are color-coded by the ammonium nitrate mass fraction.

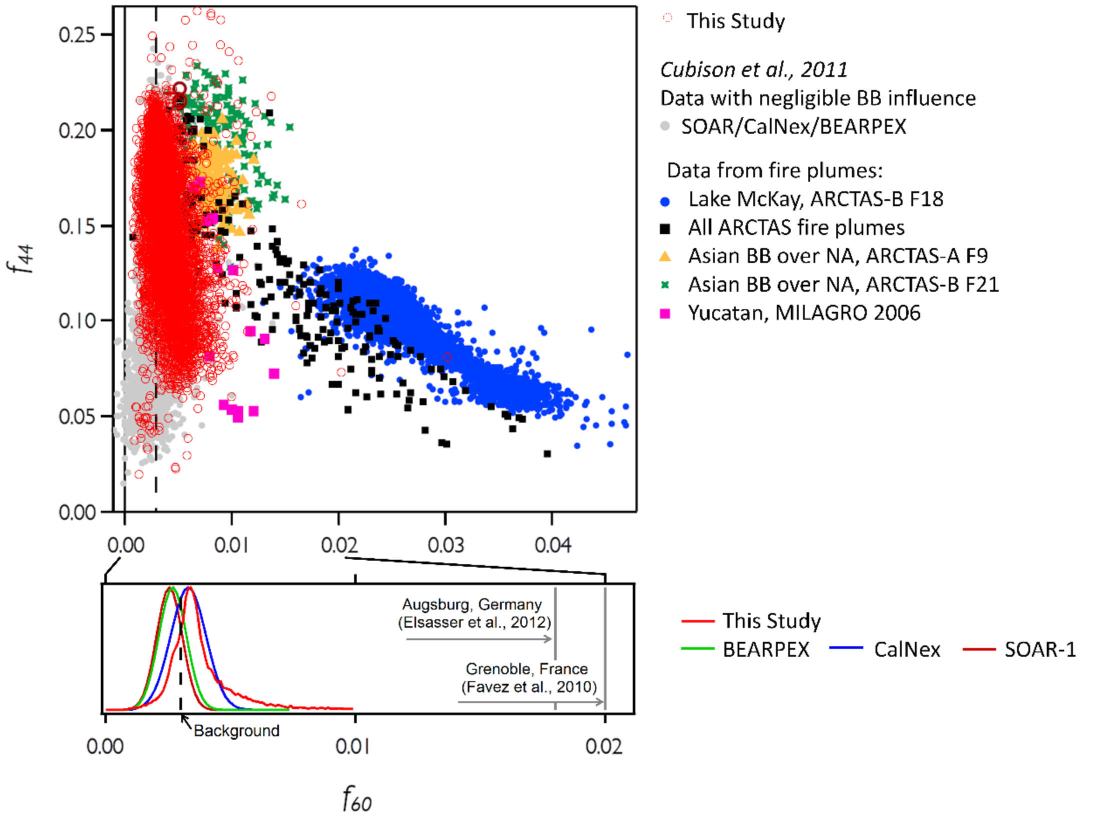

Figure 6: Top: fraction of the organic fragment at m/z = 44 divided by the total organic mass (f_{44}) as a function of the fraction of the organic fragment at m/z = 60 divided by the total organic mass (f_{60}). f_{44} and f_{60} are commonly used as markers for oxidized organic aerosol and for freshly emitted biomass burning aerosol, respectively The red open circles are the data measured during the entire UWFPS. The other symbols show data from previous studies (see Cubison el al., 2011 and references therein), with colored (non-red) points for the biomass burning (BB) plumes and grey points for data with negligible BB influence. The dashed black line corresponds to 0.003, the AMS background value for f_{60}. Bottom: frequency distribution of f_{60} values for this study (light red) and for previous studies with negligible BB influence (green, blue and dark red lines). The vertical grey solid lines show f_{60} values for locations where the influence of wood combustion on organic aerosol was strong.

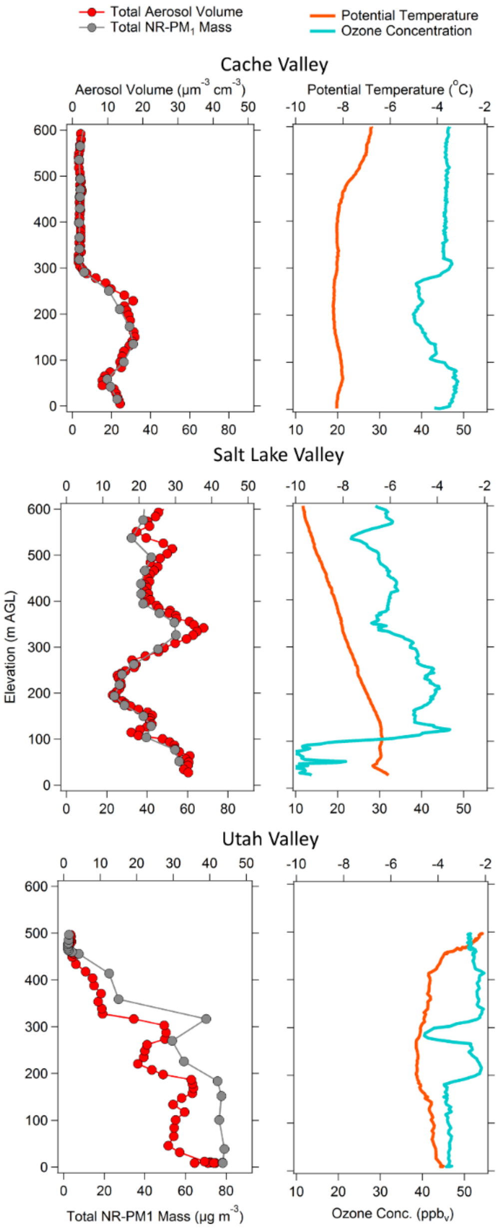
Total Aerosol Volume
Total NR-PM$_1$ Mass
Potential Temperature
Ozone Concentration
Cache Valley
Aerosol Volume (μm^{-3} cm^{-3})
Potential Temperature (°C)
0 10 20 30 40 50
-10 -8 -6 -4 -2
600 500 400 300 200 100 0
0 20 40 60 80
10 20 30 40 50
Salt Lake Valley
Elevation (m AGL)
Utah Valley
Total NR-PM1 Mass (μg m^{-3})
Ozone Conc. (ppb$_v$)

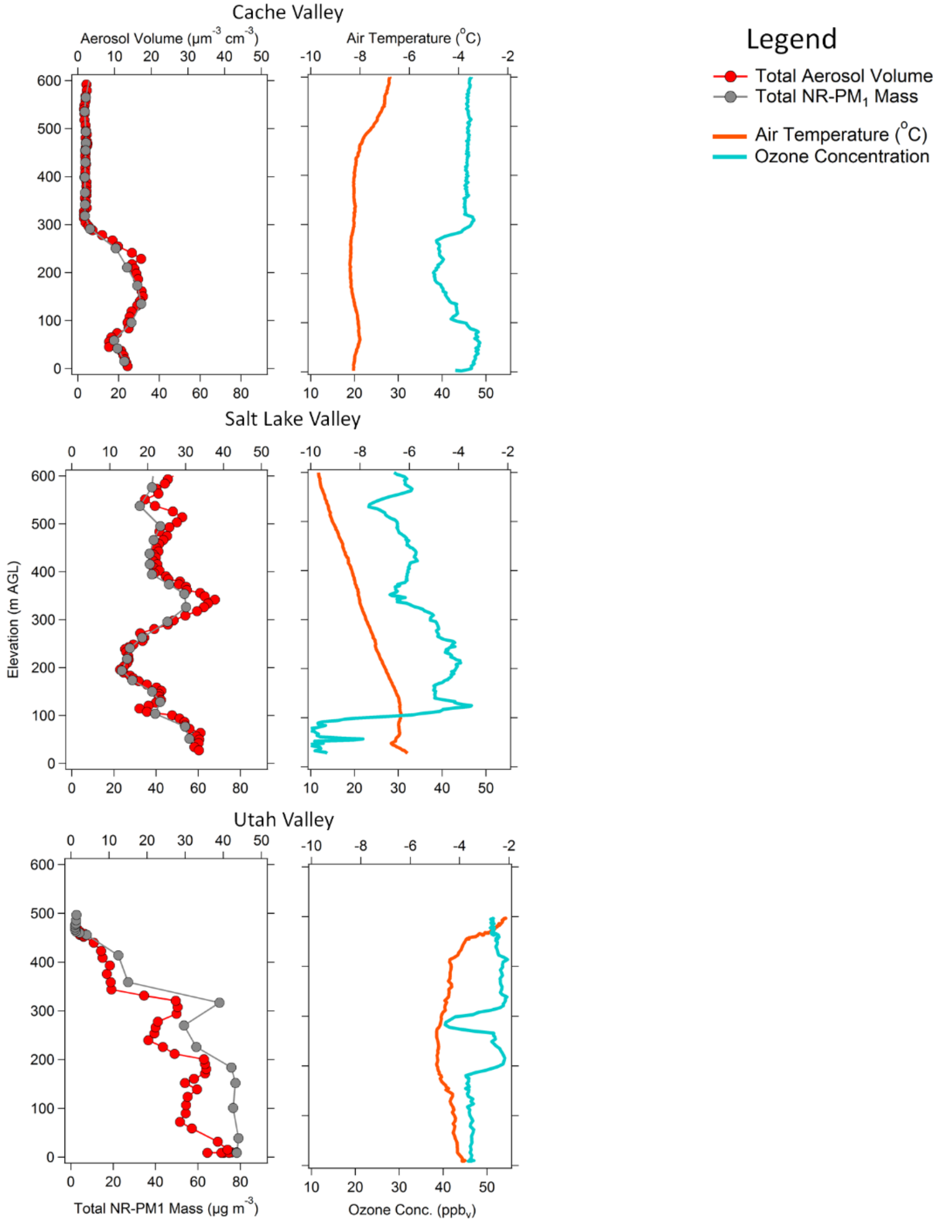

Figure 7: Comparison between selected vertical profiles. On the left is shown the aerosol volume, measured with the UHSAS (in red) and NR-PM₁ mass measured with the AMS (in grey) as function of elevation in m AGL. On the right: are shown vertical profiles of ozone concentration (light blue) and potential temperature (orange) for the same three missed approaches. The missed approach in Cache Valley took place on Jan 28 at 18:38 MST at the Logan-Cache Airport (LGU); the one in Salt Lake Valley on Jan 28 at 20:22 MST at Salt Lake City International (SLC), and the one in Utah Valley on Jan 30 at 13:24 MST at the Provo Municipal Airport (PVU).

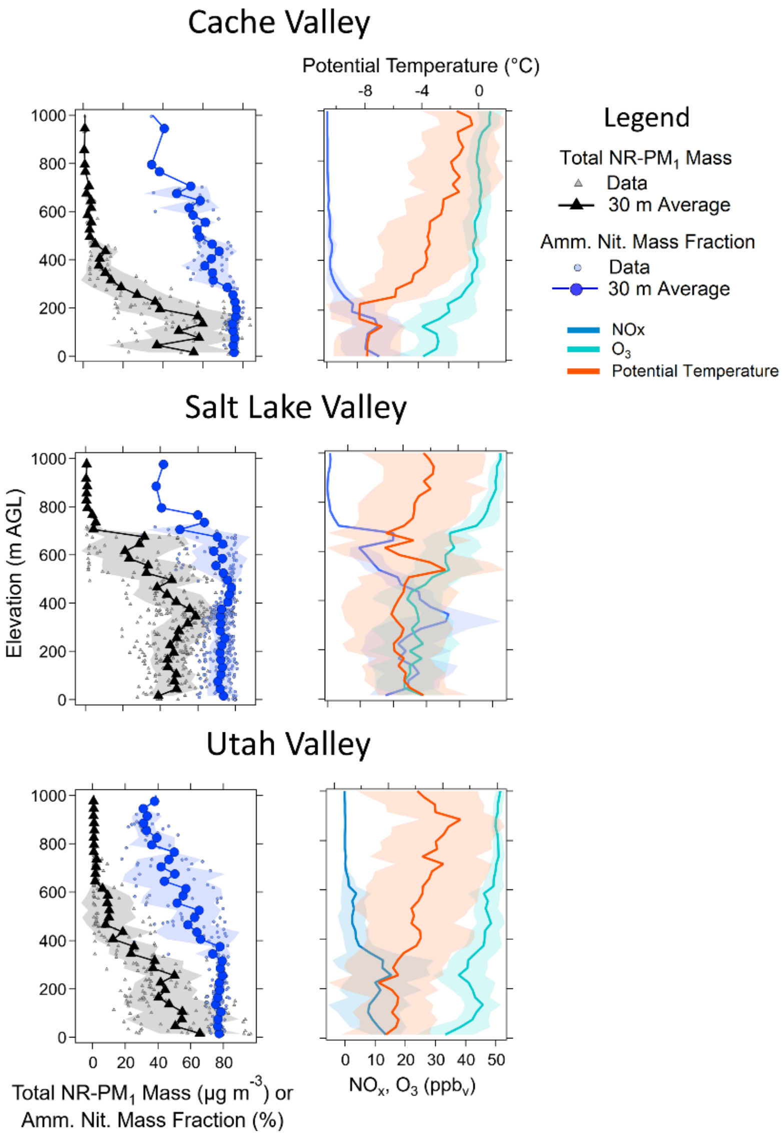
Cache Valley
Potential Temperature (°C)
-8
-4
0
Salt Lake Valley
Utah Valley
Elevation (m AGL)
1000
800
600
400
200
0
0
20
40
60
80
Total NR-PM$_1$ Mass (µg m^{-3}) or
Amm. Nit. Mass Fraction (%)
0
10
20
30
40
50
NO$_x$, O$_3$ (ppb$_v$)
Legend
Total NR-PM$_1$ Mass
Data
30 m Average
Amm. Nit. Mass Fraction
Data
30 m Average
NOx
O$_3$
Potential Temperature

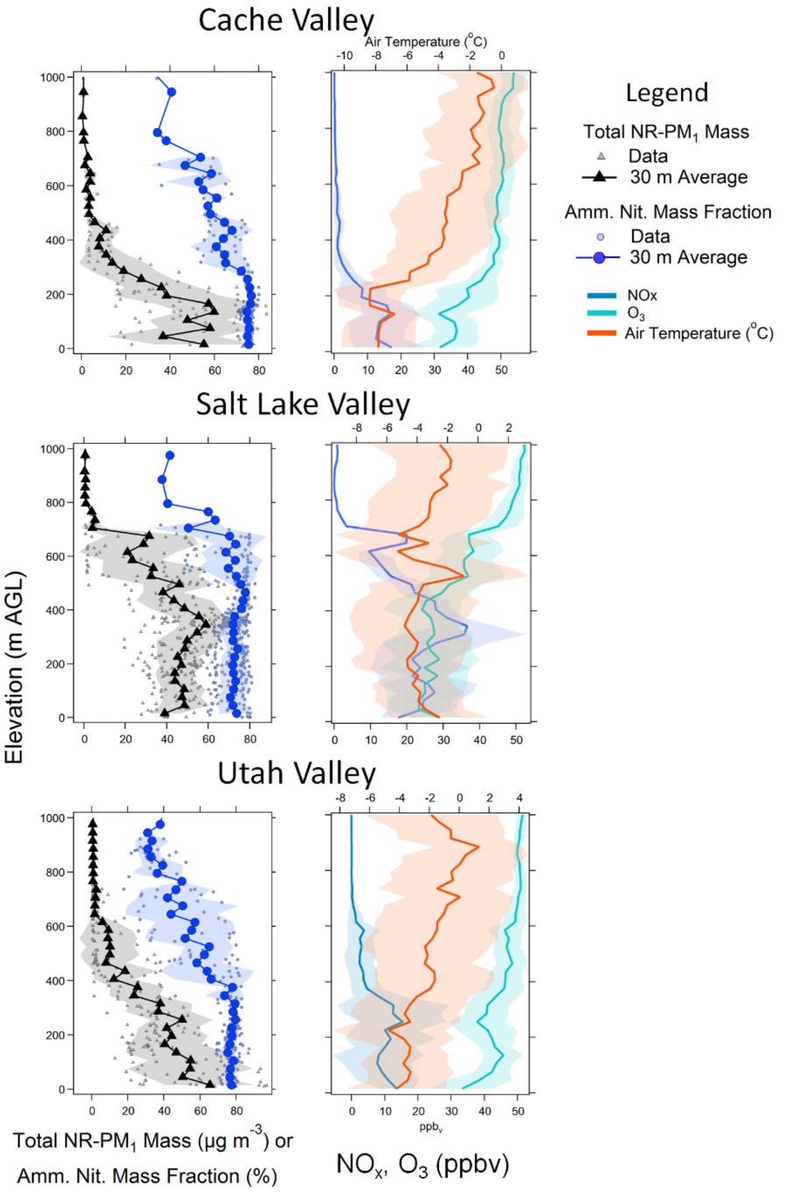

Figure 8: Left: average vertical profiles of NR-PM$_1$ mass (black triangles) and ammonium nitrate mass fraction (blue circles) measured during Episode#2. The triangular small grey markers and the small light blue circles are data used in the averages for all the missed approaches at the same airports as in Figure 7. The black triangles and dark blue circles are averages over 30 meters with their associated standard deviations. Right: corresponding vertical profiles of NO$_x$ (blue lines), O$_3$ (aqua lines) and potential temperature (orange lines).

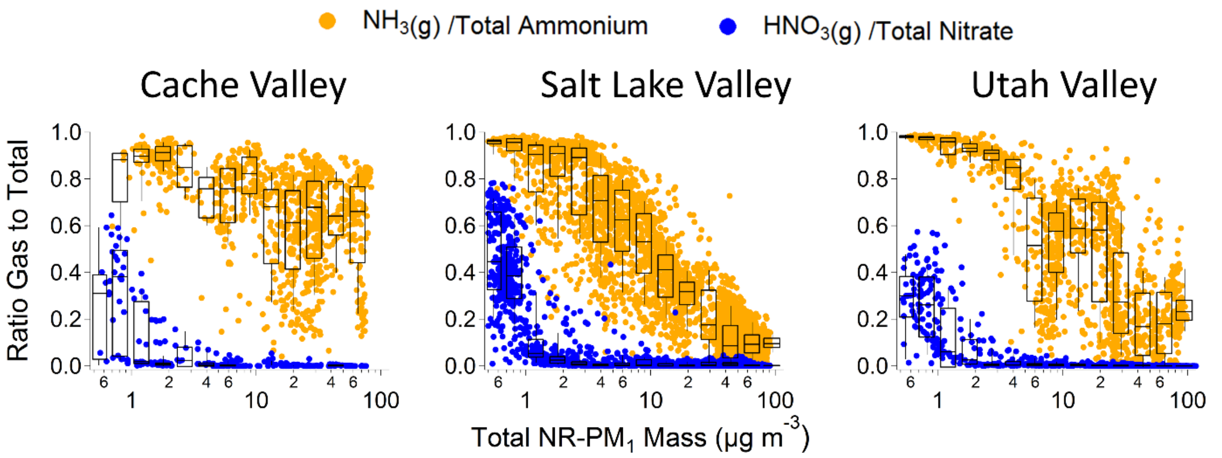

Figure 9: Fraction of gas phase species to total mass (gas + aerosol) plotted as a function of total observed aerosol mass. In orange is the ratio between gas phase ammonia NH_3 and total ammonium $NH_3(g)+NH_4^+$. In blue is the ratio between gas phase nitric acid HNO_3 and total nitrate $HNO_3 + NO_3^-$. Overlaid onto the data point are box and whiskers plots for logarithmically spaced bins. The boundary of the boxes are 25th and 75th percentiles, the line in the box is the 50th percentile and the whiskers are 10th and 90th percentiles.

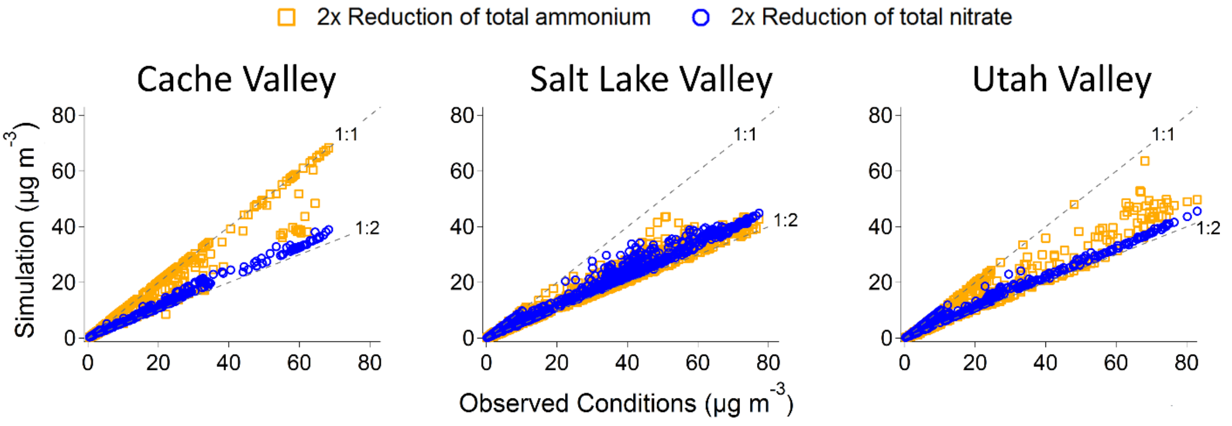

Figure 10: Comparison of the simulated total inorganic aerosol mass (y-axis) to the observed total inorganic aerosol mass with separate reductions in precursor species using ISORROPIA (x-axis). Two different scenarios are shown: a twofold reduction of total ammonium (orange) and a twofold reduction in total nitrate (blue). The dashed grey lines in each plot represent the 1:1 line (i.e. no change in the simulated total inorganic mass in the aerosol phase) and the 1:2 line (i.e. a twofold reduction in the simulated total inorganic mass in the aerosol phase).

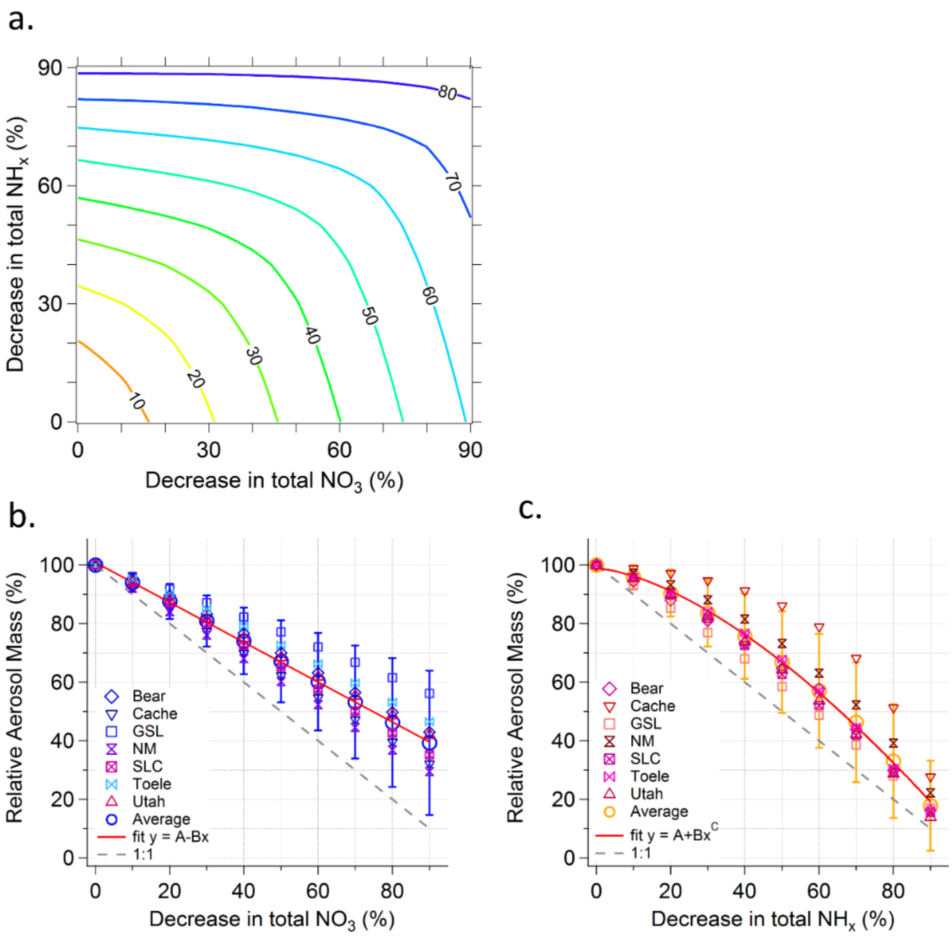

Figure 11: a) Contour plot showing the simulated decrease in total inorganic aerosol mass (contour lines, numbers shown in %) as a function of both decrease in total nitrate (x-axis) and in total ammonium (y-axis). The data inputs used here are from the entire region. The decreases are relative to the observed conditions and expressed as percentages. Panels b) and c) show one-dimensional views of the surface plot shown in panel a). Panels b) and c) are projections along the x- and y-axes respectively. b) shows the simulated decrease in total inorganic NR-PM_1 as a function of the decrease in total nitrate. In these simulations, the concentrations of total ammonium were kept constant, equal to the observed conditions. c) shows the simulated decrease in total inorganic NR-PM_1 as a function of the decrease in total ammonium. In these simulations, the concentrations of total nitrate were kept constant; equal to the observed conditions. The open circles are averages over the entire region (same as panel a.). The error bars are the standard deviations associated to the averages. The other markers are data relative to particular regions: Bear Valley, Cache Valley, the Great Salt Lake, North Metro, Salt Lake Valley, Tooele Valley and Utah Valley. The dashed grey line is the 1:1 line and the red solid lines are a fit through the average points to guide the eye (linear fit in panel b.) and power law in panel c.)).

Supplementary Information

AMS Calibrations for UWFPS

Normal procedures were used to calibrate the AMS flow rate as a function of measured lens pressure and particle time-of-flight velocity (i.e. the velocity of the aerosol particles in vacuum, from the chopper to the vaporizer) as a function of particle size [*Canagaratna et al.*, 2007]. For airborne measurements, we used a pressure-controlled inlet (PCI) that maintained a constant mass flow rate into the AMS [*Bahreini et al.*, 2008]. Because particle time of flight velocity depends on the AMS flow rate [*Bahreini et al.*, 2003], the PCI also provided a stable particle time-of-flight velocity calibration. The flow rate and velocity calibration values used for UWFPS were similar to those found for our other studies with the same AMS instrument operated with the PCI. The actual sampling pressures for both the PCI and the AMS inlet were recorded and remained constant.

For nitrate ionization efficiency (IE_{NO3}) calibrations, the ion signals from individual, size-selected, ammonium nitrate particles are used to determine the number of ions per unit mass generally in the following manner. Dry ammonium nitrate particles are formed by nebulizing a dilute aqueous solution with a custom atomizer followed by a silica gel dryer. These particles then sized with a calibrated differential mobility analyzer (DMA), ranging from about 250 nm to 500 nm in mobility diameter. Individual particle mass spectra are recorded with the AMS for at least 200 individual particle events at each size. For each particle spectrum recorded, the main nitrate ion signals at *m/z* 30 and 46 are integrated to obtain the number of nitrate ions per particle for a given mass obtained by converting the mobility diameter into volume and applying the particle density and Jayne shape factor [*Jayne et al.*, 2000]. The number of *m/z* 30 plus 46 ions per molecule of ammonium nitrate is the definition of IE_{NO3} and is subsequently used to convert ion signals from the AMS into mass units [*J.D. Allan et al.*, 2003]. This procedure relies on a narrow size range obtained from a calibrated DMA.

Here we used a slightly different procedure to determine IE_{NO3}. Instead of stepping through sizes with the DMA with a narrow size window, we increased the size range of particles transmitted through the DMA and used the AMS internal size calibration of vacuum aerodynamic diameter (d_{va}) from the particle time-of-flight velocity to calculate the particle size with the AMS. Plots of the integrated ion signals per particle (IPP) versus the cube of the vacuum aerodynamic diameter (d_{va}^3 in nm^3) are linear as shown below for calibration data obtained on 23 Jan. 2017.

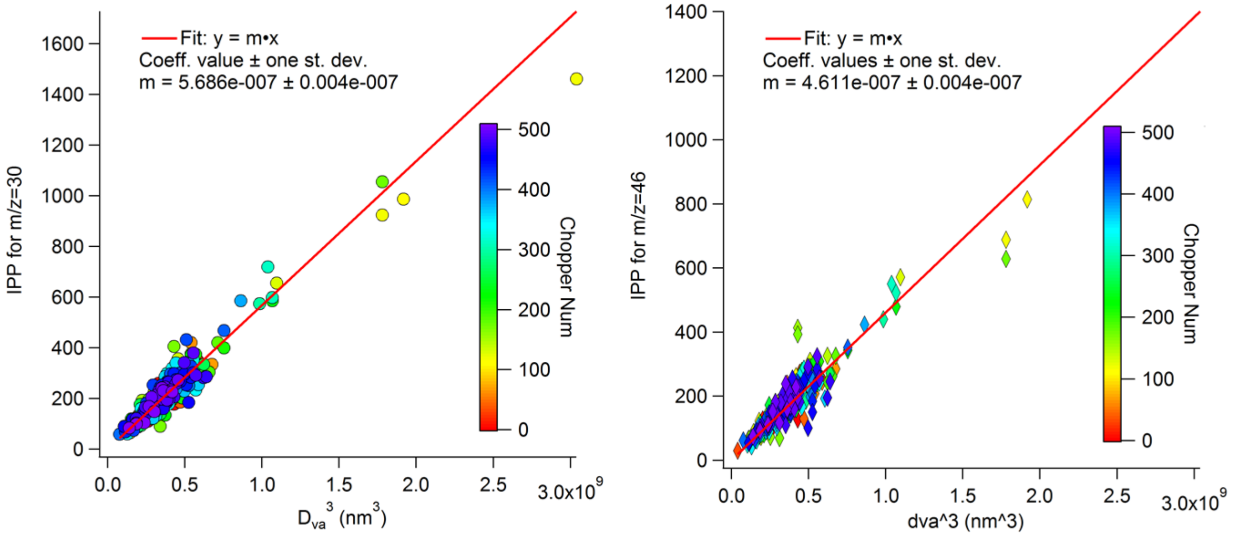

Points are colored by particle number and do not indicate any dependence with time over a wide range of particle volumes. Linear regression fits are shown with the intercept coefficients forced through zero. The vacuum aerodynamic diameter is proportional to the physical diameter times the effective density [*DeCarlo et al.*, 2004], and so the cube of the vacuum aerodynamic diameter is a measure of particle volume. Hence, d_{va}^3 for each particle can be converted into units of mass per particle. Therefore the sum of the two slopes from these plots are proportional to IE_{NO3} as follows:

$$IE_{NO3} = [IPP_{\text{slope at 30}} + IPP_{\text{slope at 46}}] \times 6/\pi \times MW_{NH4NO3} \times (s \times \rho_{NH4NO3})^2 / (N_A\ \rho_0^3\ 10^{-21}) \qquad (1)$$

where the value of 10^{-21} is a unit conversion factor for nm^3 to cm^3. Using the molecular weight of ammonium nitrate (MW_{NH4NH3} = 80 g mol^{-1}), the Jayne shape factor for ammonium nitrate (s = 0.8 [*Jayne et al.*, 2000]), the density of dry ammonium nitrate (ρ_{NH4NO3} = 1.72 g cm^{-3} [*Perry and Green*, 1997]), Avogadro's number (N_A = 6.022e23 molec mol^{-1}), standard density (ρ_0 = 1 g cm^{-3}), and π = 3.14, this equation simplifies to:

$$IE_{NO3} = [IPP_{\text{slope at 30}} + IPP_{\text{slope at 46}}] \times 0.48 \qquad (2)$$

where IE_{NO3} is in units of ions per molecule. This procedure eliminates issues with calibrating the DMA and has the advantage of using the internal AMS sizing calibration to independently determine IE_{NO3}.

For IE_{NO3} calibrations encompassing the entire UWFPS study, we found that the ratio of IE_{NO3} to the airbeam signal at *m/z* 28 (AB) was linear over a wide range of sensitivities.

$$IE_{NO3} = 1.167e\text{-}12 \times AB - 2.06e\text{-}7 \qquad (3)$$

This equation was used to calculate IE_{NO3} for a reference AB value at the beginning of each set of flights on a given day.

The relative ionization efficiency of ammonium (RIE_{NH4}) was determined from all of the ammonium nitrate calibration data by forcing the number of moles from the measured ammonium ion signals equal to the number of moles from the measured nitrate ion signals for the ammonium nitrate particles. It had a slight time dependence over the course of the study, decreasing from 4.46 on 31 Dec. 2016 to 3.44 on 2 Feb. 2017.For the final calibration on 10 Feb. 2017, RIE_{NH4} was 3.42.

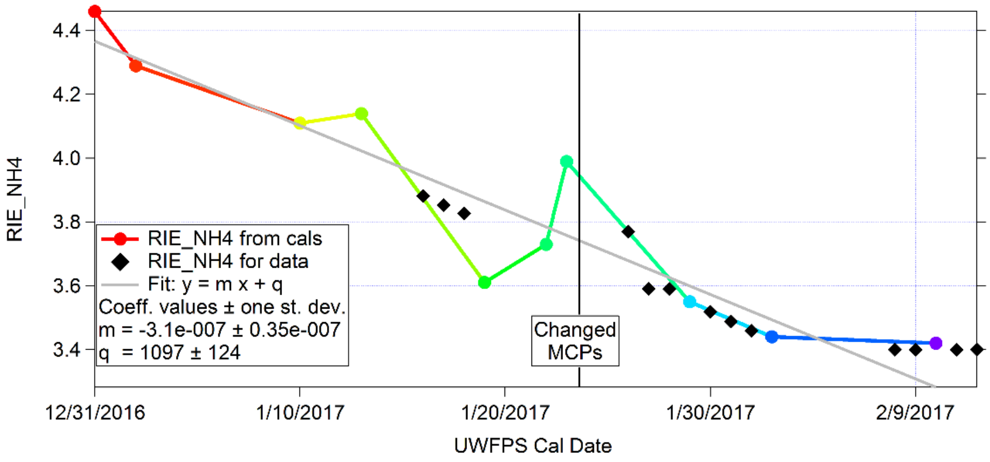

This time dependence in the RIE_{NH4} calibrations (colored points) was fit to the following equation (grey line above):

$$RIE_{NH4} = -3.0636e\text{-}7 \times (\text{date in seconds}) + 1097 \qquad (4)$$

and used for the UWFPS data with the minimum RIE_{NH4} for the last 4 flights fixed at 3.4.

If complete ion balance is assumed for the ambient UWFPS measurements (during polluted conditions the inorganic $NR\text{-}PM_1$ composition was mostly ammonium nitrate, see Figures 3, 4, S6, and S7), an implied RIE_{NH4} can be determined from the field data (black diamonds above). The overall trend in time for RIE_{NH4} measured from the calibrations was clearly evident in the ambient data and the nearly constant RIE_{NH4} of 3.4 at the end of the study was seen in both the calibrations and ambient data. Even a slightly higher

RIE_{NH4} was reflected in the ambient data for the flight directly after changing the microchannel plate detectors (MCPs) in the middle of the study. Thus, this careful calibration of RIE_{NH4} demonstrates the overall ion balance to within a few percent in the UWFPS dataset (see Figure 5 in the main text).

For the final calculation of the mass concentrations, the collection efficiency (CE) must be determined [*J. D. Allan et al.*, 2004; *Matthew et al.*, 2008]. Here the bulk inorganic speciation was used to initially estimate CE using the algorithm based on prior field data [*Middlebrook et al.*, 2012], and indicated that it should be less than one for most of this dataset. However, the instrument used for this study has a light scattering (LS) module to measure the in situ CE of particles that are large enough to scatter light [*Liao et al.*, 2017]. We operated the instrument in the light scattering single particle mode for 30 s every 5 minutes. During time periods where significant mass concentrations of ammonium nitrate were measured, the in situ CE from light scattering was closer to 1 than indicated from the CE algorithm. Because CE from the LS counts was closer to 1 and CE for pure, dry ammonium nitrate equals 1 [*Matthew et al.,* 2008], we used CE = 1 for most of this dataset.

There is some uncertainty in CE for the smallest mass concentrations, where the particle counting statistics were not high enough to reliably use the in situ CE from light scattering data. The mass fraction data as a function of total AMS mass indicated that the composition was clearly different than for the higher total mass concentrations (see Figure 3, 4 and S5), and the CE could potentially also be different. There is also uncertainty in the CE for data points where the refractory chloride mass fraction was relatively high, typically for measurements around the magnesium plant on the southwestern side of the Great Salt Lake. For those data points with low total mass concentrations or high chloride mass fractions, we assumed that the CE was also equal to 1. However, the true CE could be as low as 0.3. Hence, the mass concentrations in the data archive for these data points should be considered a lower limit and could actually be as much as a factor of 2 or 3 larger than reported.

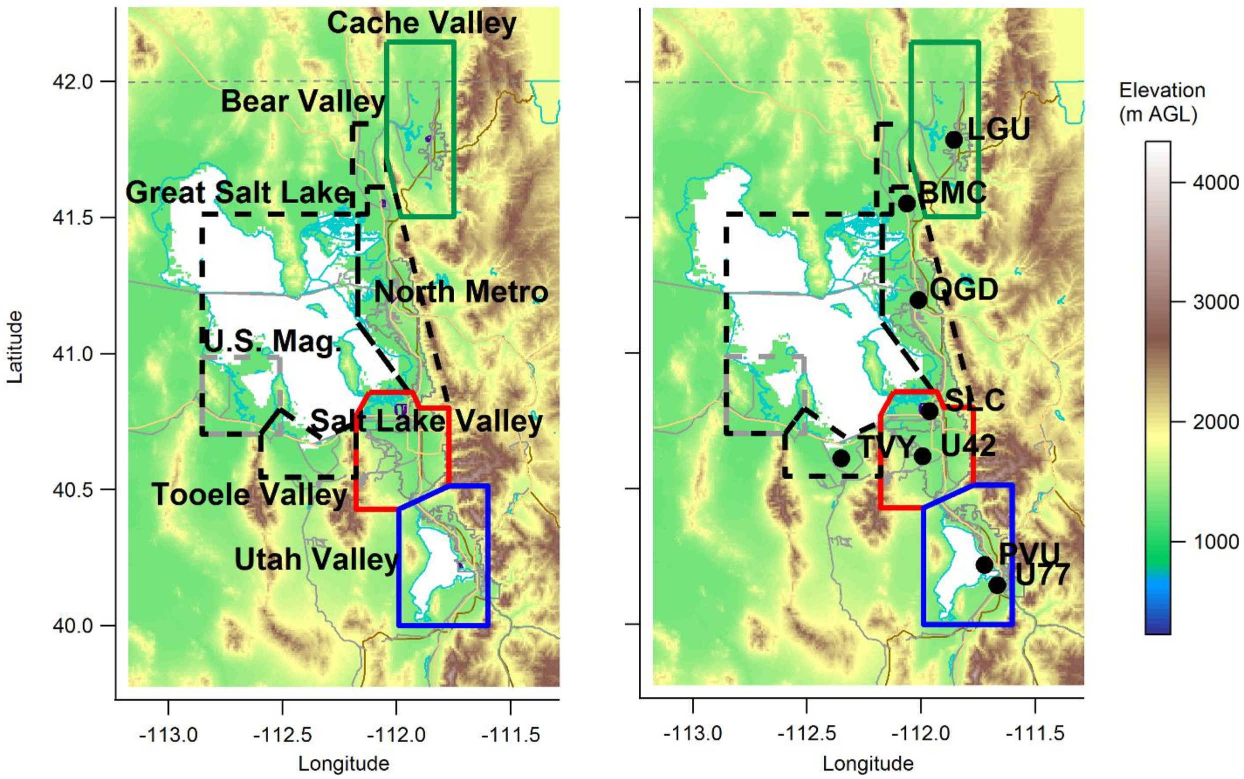

Figure S1. Maps of the area of interest for our study. Left: Outlines of the boundaries for the regions considered in our analysis. From north to south: Cache Valley, Bear Valley, Great Salt Lake, North Metro, U.S. Magnesium plant, Salt Lake Valley, Tooele Valley and Utah Valley. Right: location of the airports where we performed missed approaches in order to measure vertical profiles. From north to south and from left to right: Logan-Cache Airport (LGU), Brigham City Airport (BMC), Ogden-Hinckley Airport (OGD), Salt Lake City International Airport (SLC), Tooele Valley Airport (TVY), South Valley Regional Airport (U42), Provo Municipal Airport (PVU) and Spanish Fork Springville (U77). The dashed lines are the same boundaries of the air basins as the left panel.

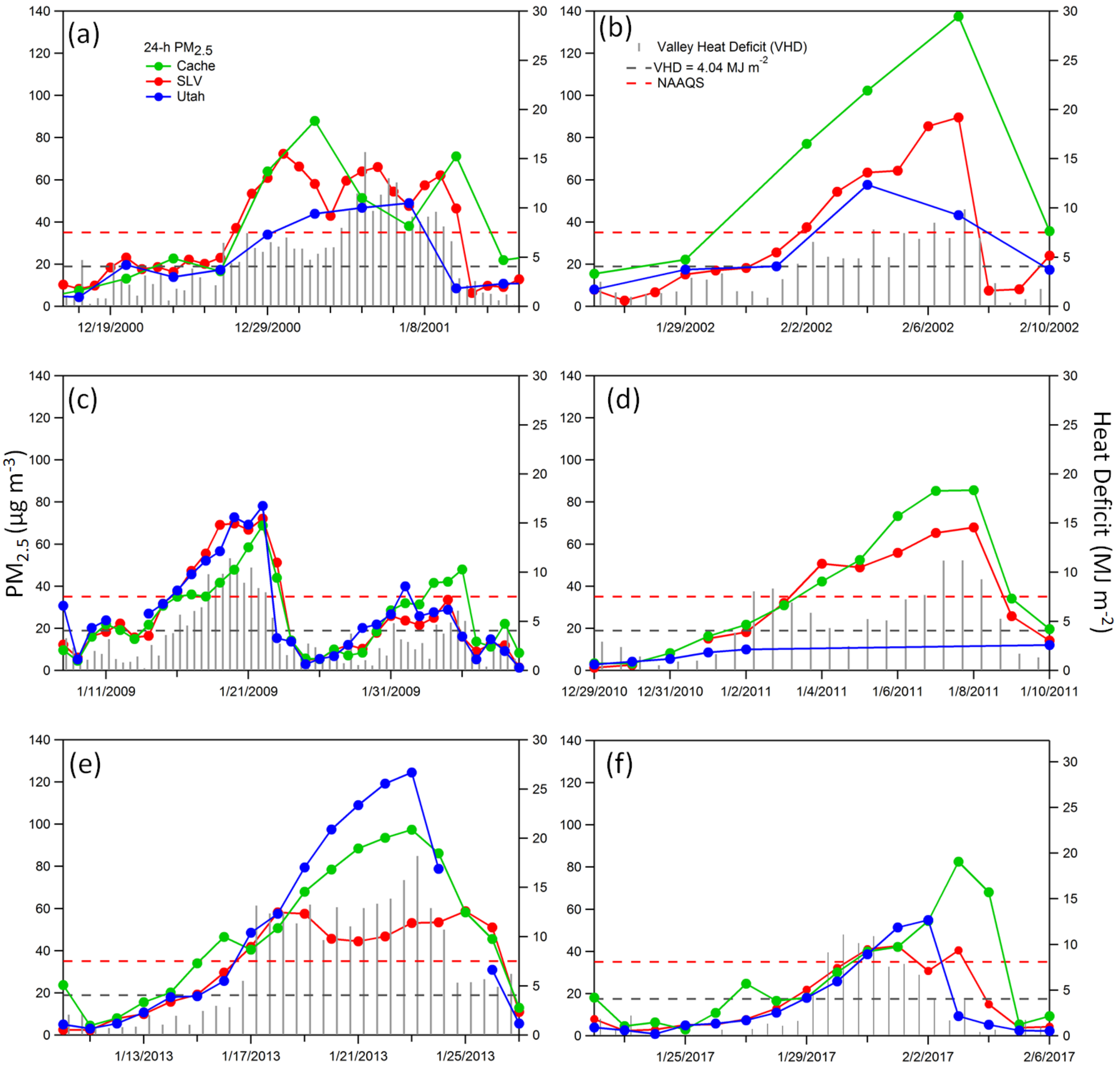

Figure S2. Examples showing the evolution of $PM_{2.5}$ during the winter with long-lasting episodes that occurred in years prior to UWFPS (a to e) and during UWFPS (f). The grey sticks are the valley heat deficit (VHD) values calculated following **Whiteman et al.** (2014), using data from balloon soundings at the Salt Lake City International Airport. High VHD values are characteristic of persistent cold air pools (PCAPs), where pollutants are trapped near the ground. The grey dashed horizontal lines are the threshold of 4.04 MJ m^{-2} (**Whiteman et al. 2014**) and the red dashed horizontal lines are the National Ambient Air Quality Standard (NAAQS) for 24-h average $PM_{2.5}$

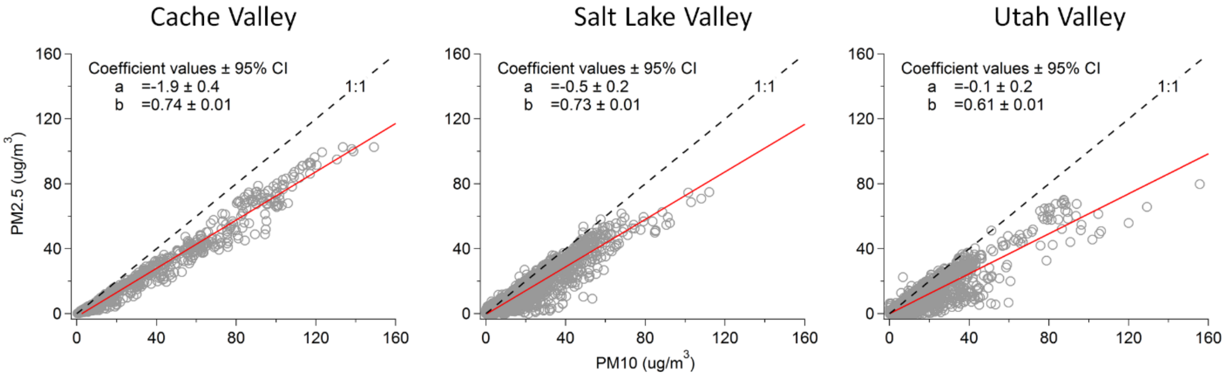

Figure S3. Comparison between hourly PM_{10} and $PM_{2.5}$ for three of the locations considered in this study. Left: Cache Valley, data from the Logan L4 site (Environmental Protection Agency). Center: Salt Lake Valley, data from the Hawthorn site (Utah Division of Air Quality –UDAQ). Right: Utah Valley, data from the North Provo site (UDAQ). The grey dashed lines are the 1:1 line; the red solid lines are linear fit. At the top of each graph are the intercepts (a) the slopes (b) from linear fits, with 95% confidence intervals (CI).

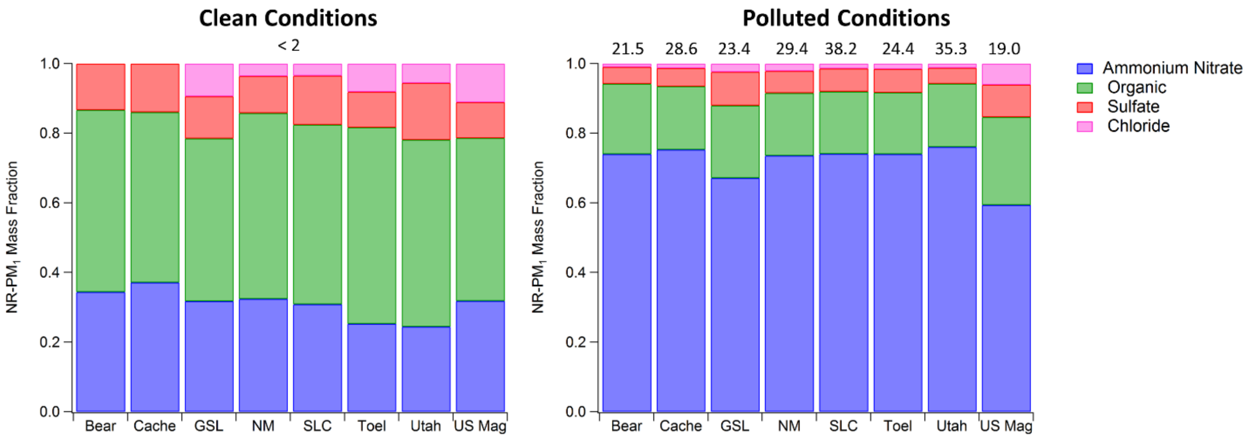

Figure S4. Average aerosol chemical composition (calculated as non-refractory PM_1 mass fraction) measured during UWFPS outside pollution events (i.e., when the total mass was less than 2 µg m^{-3}–left) and during pollution events (i.e., when the total mass was greater than 17.5 µg sm^{-3}–. The values above the pie charts are median concentrations for polluted conditions over the entire period of the UWFPS.

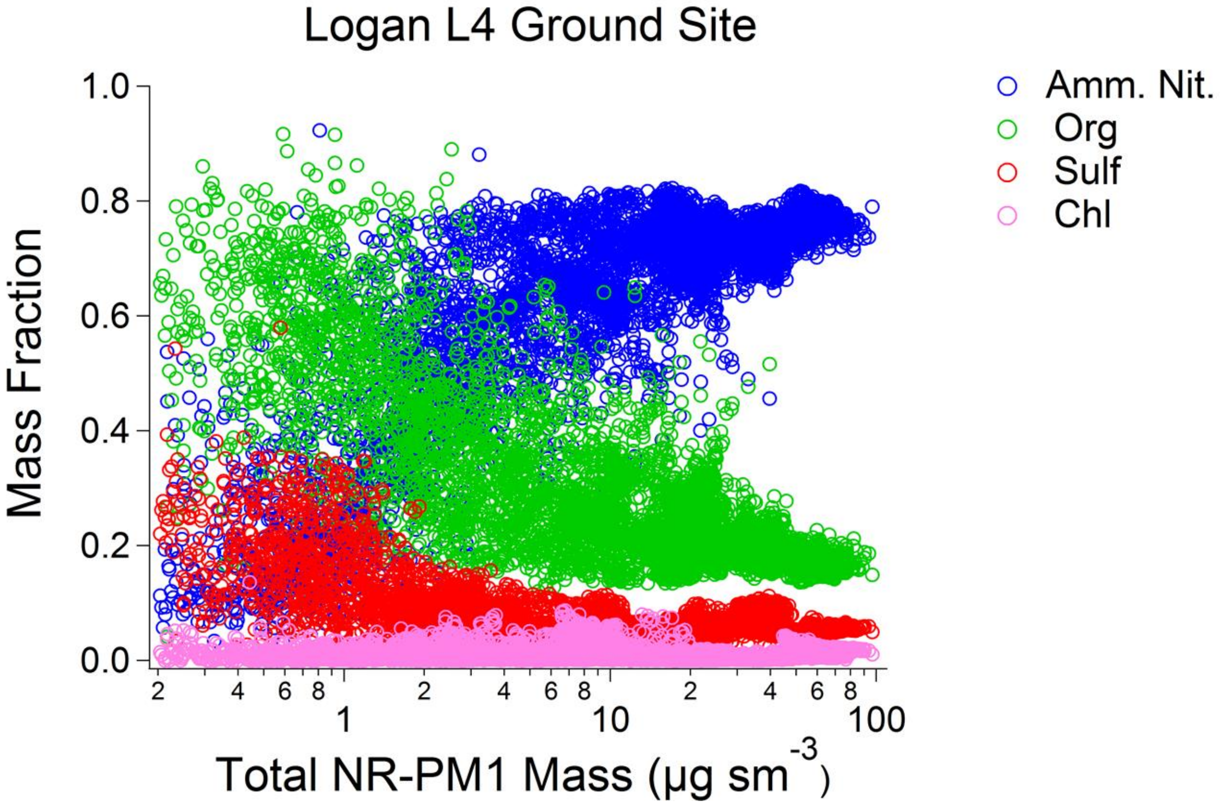

Figure S5. Aerosol mass fraction as a function of the total mass of NR-PM$_1$. Data from the AMS located at the Logan L4 ground site. The mass fraction of ammonium nitrate is in blue, of organic in green, of sulfate and chloride in red and pink, respectively.

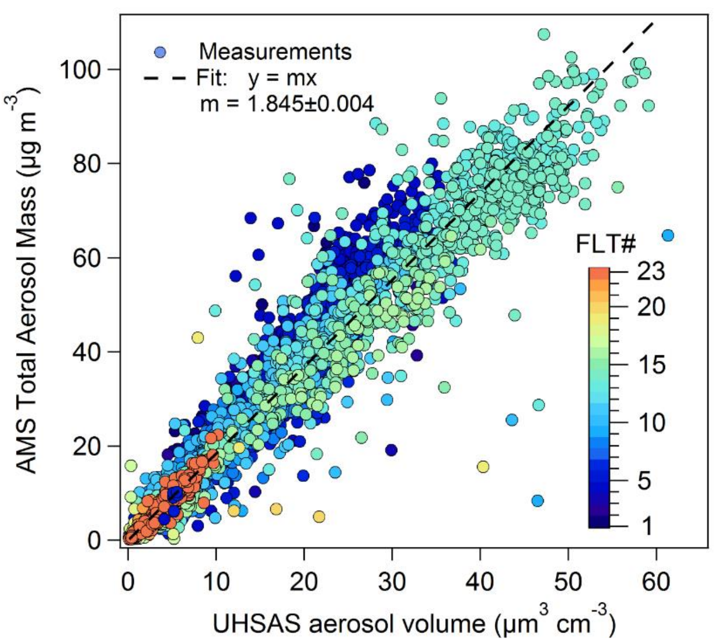

Figure S6. Comparison between the total aerosol mass in µg m^{-3}, measured with the AMS and the aerosol volume in µm^3 cm^{-3}, measured with the UHSAS. The black dashed line is a fit through the data. The slope, *m* = 1.85, is within experimental error compatible with the density of ammonium nitrate (1.72 g cm^{-3}, **NIST Chemistry WebBook**). Color-coded is the flight number.

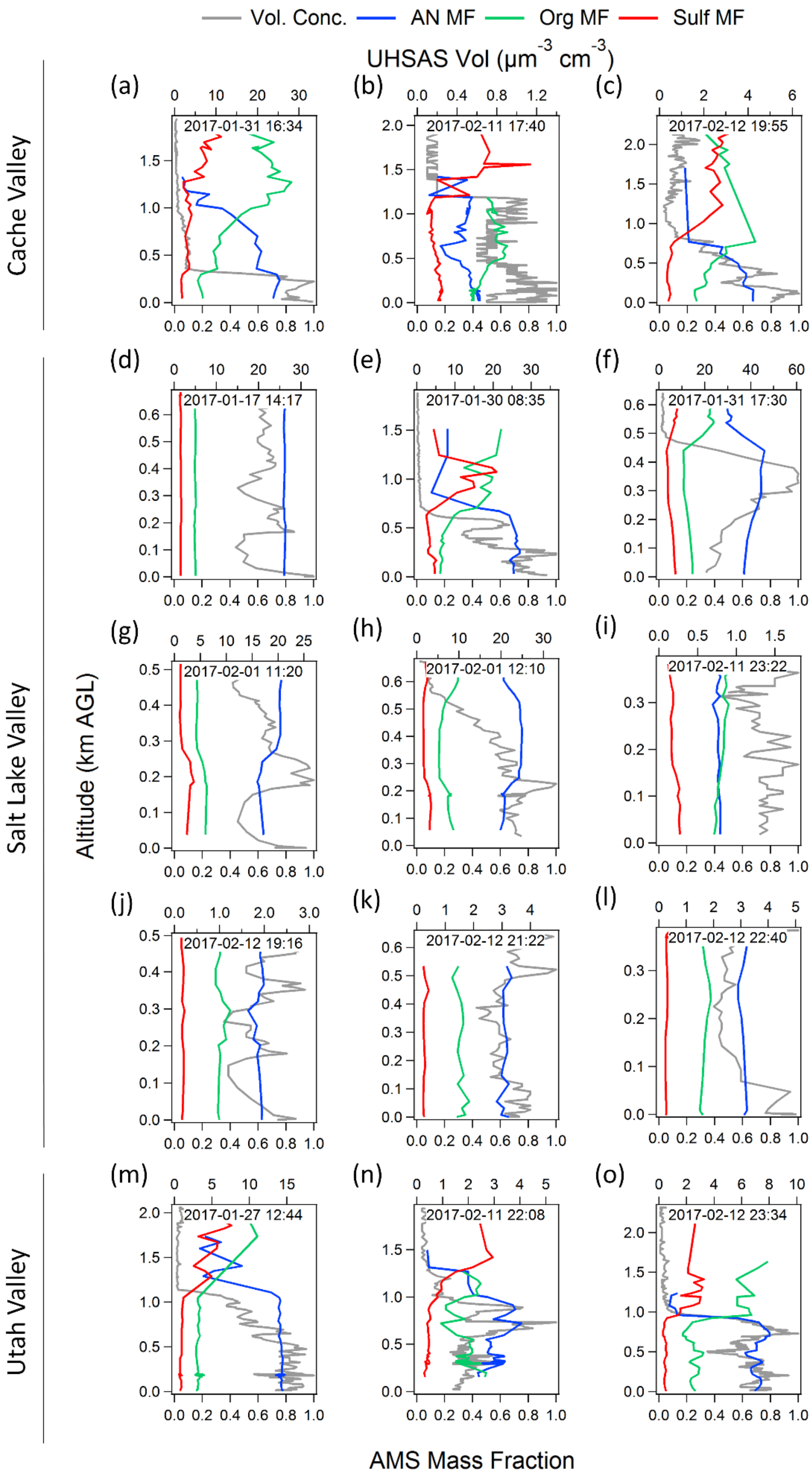

Figure S7. Various vertical profiles of aerosol volume (top axis) and aerosol NR-PM$_1$ mass fraction (bottom axis) for Cache Valley, Salt Lake valley and Utah Valley.

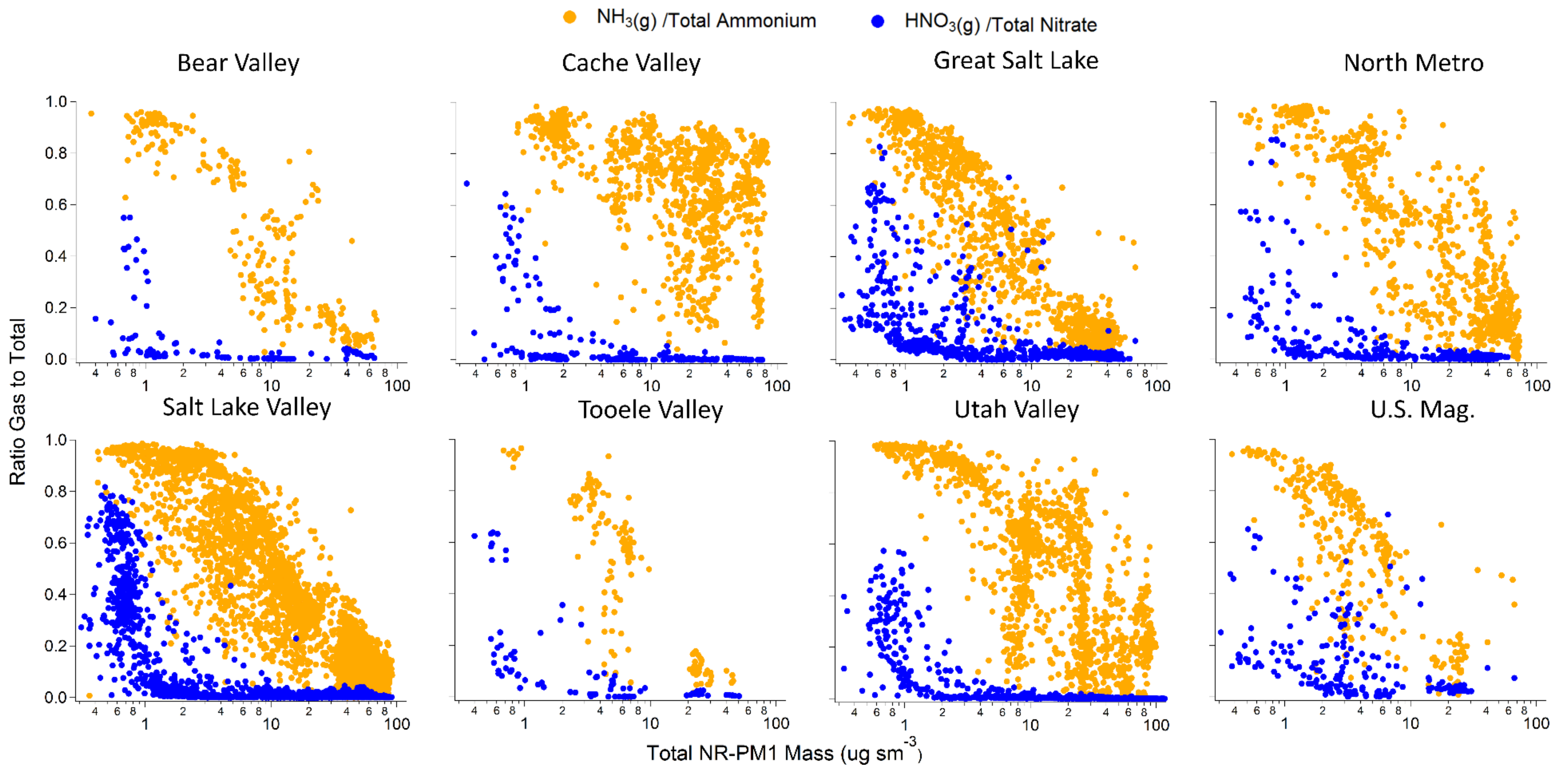

Figure S8. Fraction of gas phase species to total mass (gas + aerosol) plotted as a function of total aerosol mass. Same as figure 9 in the main text, only for all the regions.

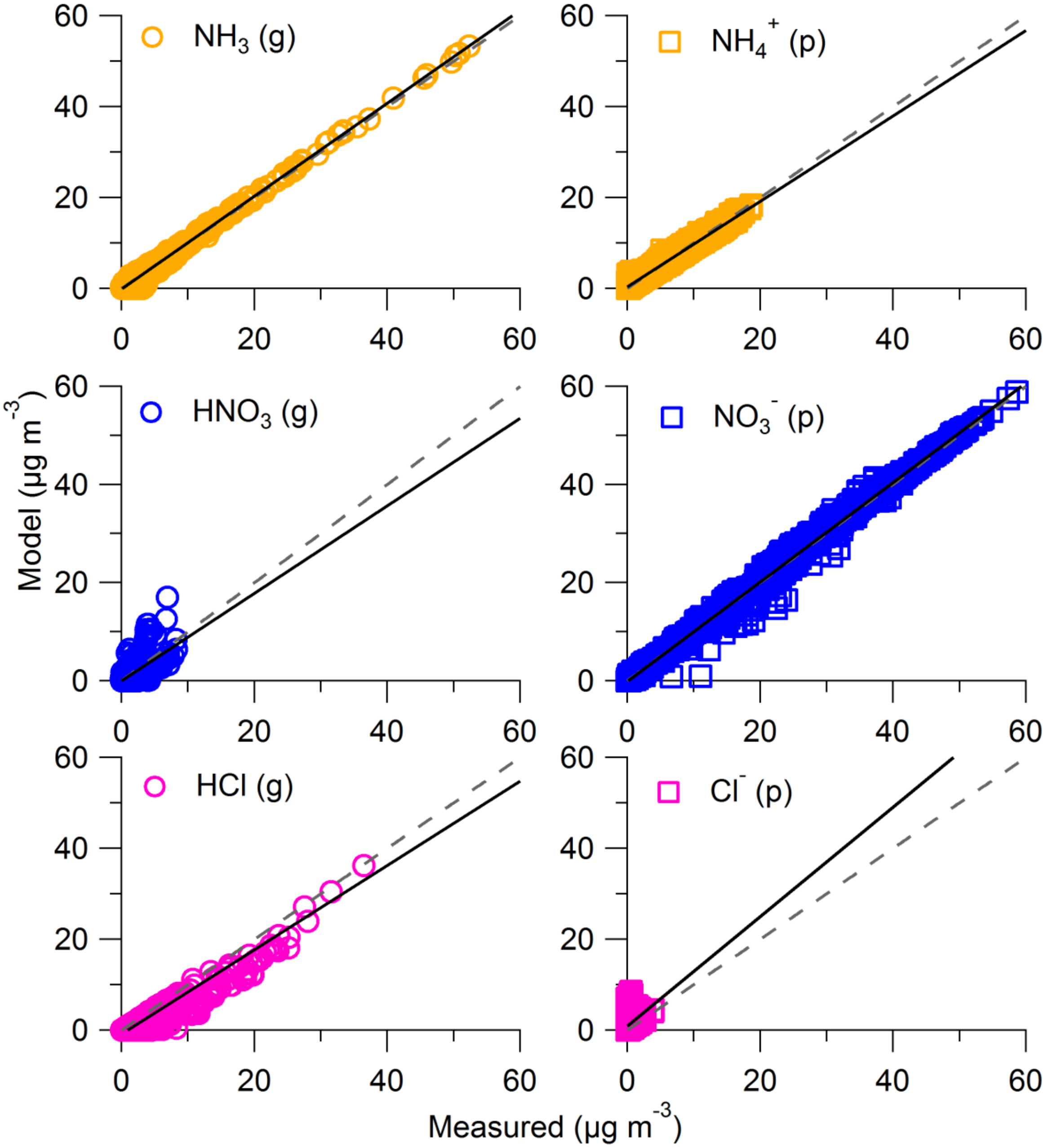

Figure S9. Comparison between measurements and ISORROPIA model output. The gas phase species denoted by "(g)", are in the left column and the particle phase species, denoted by "(p)", are in the right column. Ammonia (NH_3) and ammonium (NH_4^+) are in yellow at the top, nitric acid (HNO_3) and nitrate (NO_3^-) are in blue at the center, hydrochloric acid (HCl) and chloride (Cl^-) are in pink at the bottom. The grey dashed line is the 1:1 line, the solid black lines are linear regressions (see Table S1 for the coefficients).

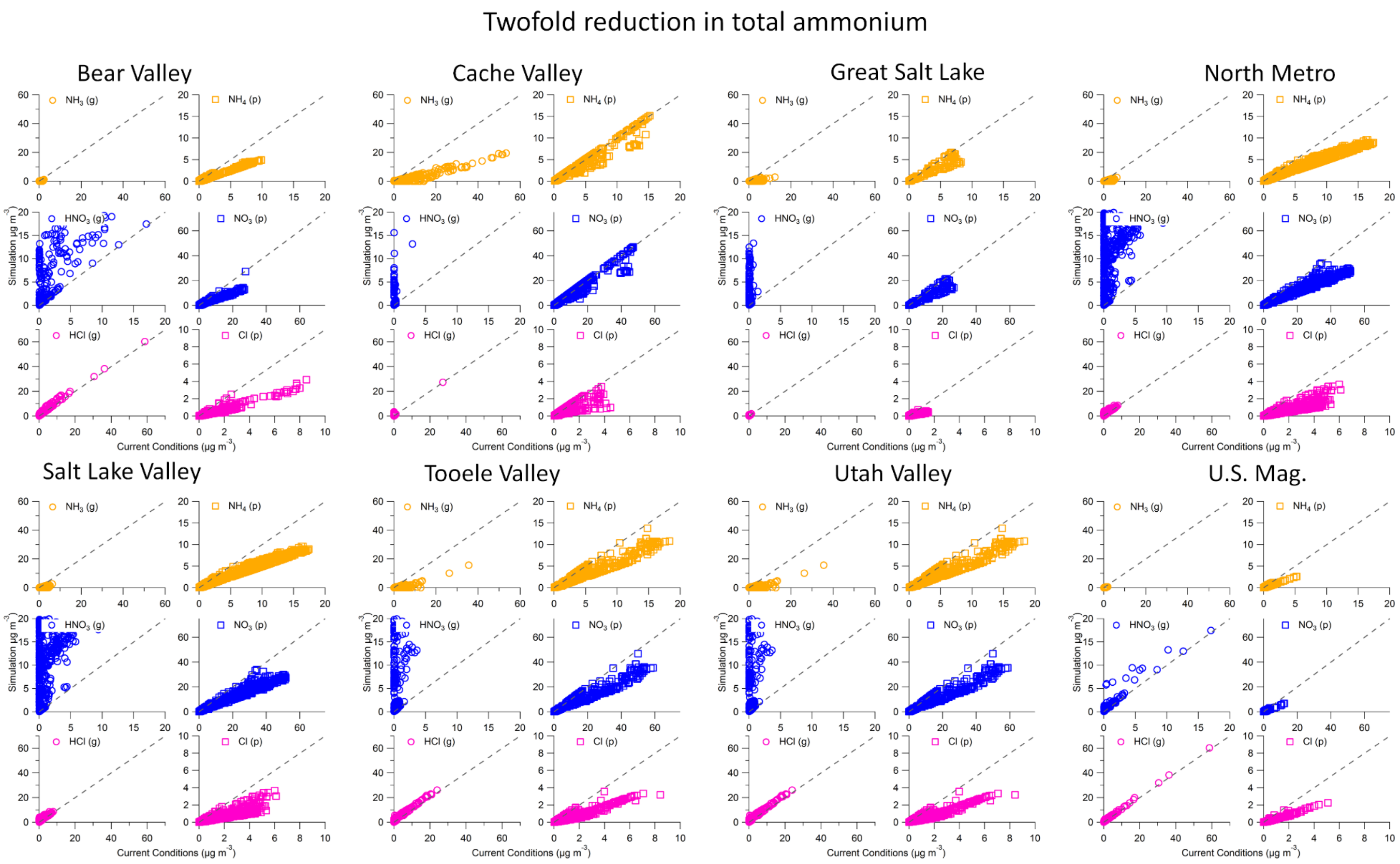

Figure S10. ISORROPIA model outputs of inorganic species for simulations using 50% decreases in total ammonium inputs from the UWFPS measurements (y-axis) compared to the corresponding model outputs using the current measured inputs (x-axis). For each location, the data are plotted in the same way as for Figure S10 (i.e., gas phase in the left column and particle phase in the right column, with ammonium, nitrate and chloride species in yellow, blue and pink, respectively).

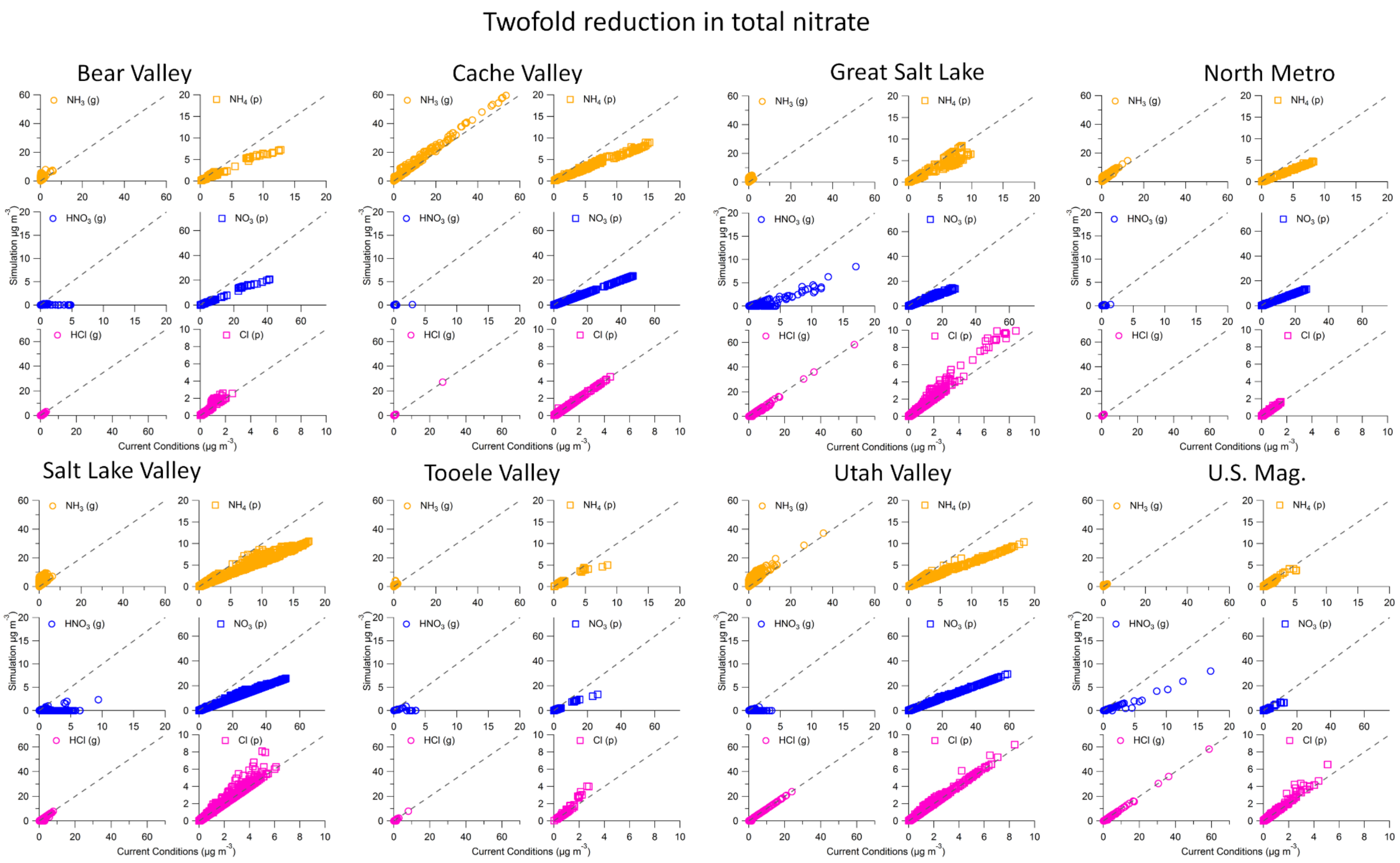

Figure S11. Same as for Figure S11, except the simulations are using 50% decreases in total nitrate inputs instead of decreases in total ammonium inputs. All locations respond to a decrease in total nitrate, indicating that inorganic aerosol formation in the region is predominantly nitrate limited.

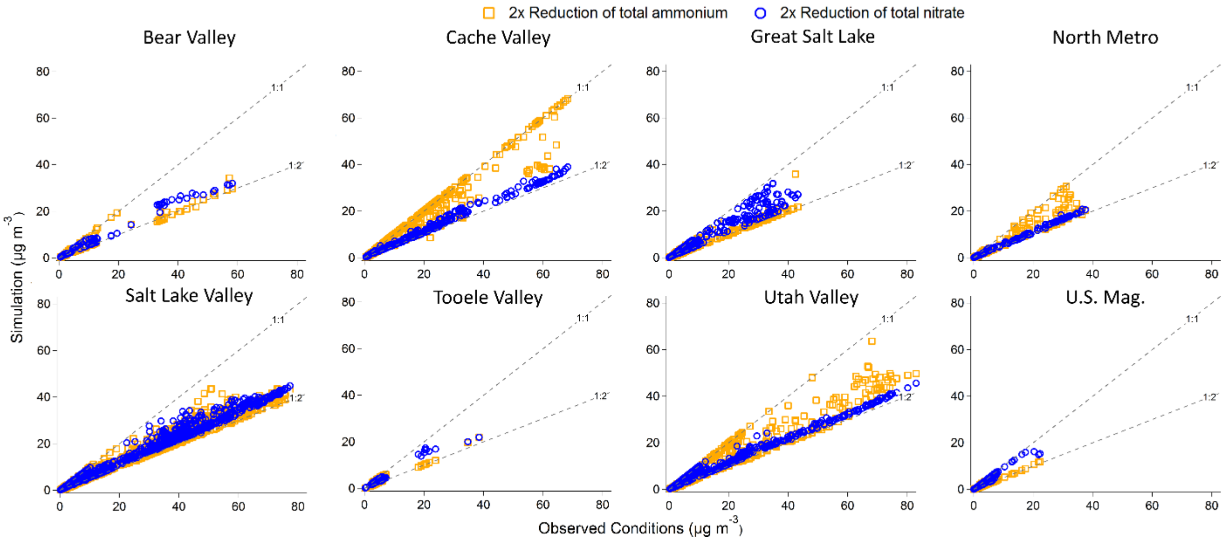

Figure S12 Comparison of the current total inorganic aerosol mass (x-axis) and the total inorganic aerosol mass simulated using ISORROPIA (y-axis). Same as Figure 11 in the main text, but shown for all the locations.

Table S1. Coefficient values for the linear regressions shown in figure S11

	Coefficient values				
Chemical Species	a	b	σ_a	σ_b	r^2
NH3	-0.14	1.023	0.01	0.003	0.983
HNO3	0.00	0.892	0.03	0.019	0.555
HCl	-0.86	0.927	0.02	0.004	0.962
NH4+	0.36	0.941	0.02	0.002	0.985
NO3-	-0.11	1.013	0.02	0.001	0.997
Cl-	0.95	1.203	0.03	0.056	0.161

References:

Allan, J. D., et al. (2003), Quantitative sampling using an Aerodyne aerosol mass spectrometer 2. Measurements of fine particulate chemical composition in two U.K. cities, *J. Geophys. Res.*, *108*(D3), 4091.

Allan, J. D., et al. (2004), A generalised method for the extraction of chemically resolved mass spectra from Aerodyne aerosol mass spectrometer data, *Journal of Aerosol Science*, *35*(7), 909-922.

Bahreini, R., J. L. Jimenez, J. Wang, R. C. Flagan, J. H. Seinfeld, J. T. Jayne, and D. R. Worsnop (2003), Aircraft-based aerosol size and composition measurements during ACE-Asia using and Aerodyne aerosol mass spectrometer, *J. Geophys. Res.*, *108*(D23), 8645, doi: 8610.1029/2002JD003226.

Bahreini, R., E. J. Dunlea, B. M. Matthew, C. Simons, K. S. Docherty, P. F. DeCarlo, J. L. Jimenez, C. A. Brock, and A. M. Middlebrook (2008), Design and operation of a pressure-controlled inlet for airborne sampling with an aerodynamic aerosol lens, *Aerosol Sci. Technol.*, *42*(6), 465-471.

Canagaratna, M. R., et al. (2007), Chemical and microphysical characterization of ambient aerosols with the Aerodyne aerosol mass spectrometer, *Mass Spectrometry Reviews*, *26*(2), 185-222.

DeCarlo, P. F., J. G. Slowik, D. R. Worsnop, P. Davidovits, and J. L. Jimenez (2004), Particle morphology and density characterization by combined mobility and aerodynamic diameter measurements. Part 1: Theory, *Aerosol Sci. Technol.*, *38*(12), 1185–1205.

Jayne, J. T., D. C. Leard, X. Zhang, P. Davidovits, K. A. Smith, C. E. Kolb, and D. R. Worsnop (2000), Development of an aerosol mass spectrometer for size and composition analysis of submicron particles, *Aerosol Science and Technology*, *33*(1-2), 49-70.

Liao, J., C. A. Brock, D. M. Murphy, D. T. Sueper, A. Welti, and A. M. Middlebrook (2017), Single-particle measurements of bouncing particles and in situ collection efficiency from an airborne aerosol mass spectrometer (AMS) with light-scattering detection, *Atmospheric Measurement Techniques*, *10*, 1-20.

Matthew, B. M., A. M. Middlebrook, and T. B. Onasch (2008), Collection efficiencies in an Aerodyne aerosol mass spectrometer as a function of particle phase for laboratory generated aerosols, *Aerosol Science and Technology*, *42*(11), 884-898.

Middlebrook, A. M., R. Bahreini, J. L. Jimenez, and M. R. Canagaratna (2012), Evaluation of composition-dependent collection efficiencies for the Aerodyne aerosol mass spectrometer using field data, *Aerosol Science and Technology*, *46*(3), 258-271.

Perry, R. H., and D. W. Green (Eds.) (1997), *Perry's Chemical Engineers' Handbook*, Table 2-37 pp., McGraw-Hill, New York, NY.